ELSEVIER

Optical Remote Sensing of Vegetation: Modeling, Caveats, and Algorithms

R. B. Myneni,[*] S. Maggion,[**] J. Iaquinta,[**] J. L. Privette,[†] N. Gobron,[**] B. Pinty,[**] D. S. Kimes,[*] M. M. Verstraete,[††] and D. L. Williams[*]

The state-of-the-art on radiative transfer modeling in vegetation canopies and the application of such models to the interpretation and analysis of remotely sensed optical data is summarized. Modeling of top-of-the-atmosphere and top-of-the-canopy radiance field is developed as boundary value problems in radiative transfer. The parameterization of the constituent functions with simple models and/or empirical data is outlined together with numerical solution methods and examples of results of model validation. Caveats in the assignment of signal characteristics to surface properties are itemized and discussed with example results. Algorithms to estimate surface properties from remote observations are classified as spectral vegetation indices, model inversion, expert systems, neural networks, and genetic algorithms. Their applicability is also discussed.

I. INTRODUCTION

The interpretation of remotely sensed reflectance data and the apportioning of signal characteristics to target properties requires an understanding of how the various physical mechanisms interact to produce the measured signal. For instance, in the application of satellite remote sensing to vegetation, an understanding of the spectral response resulting from leaf internal microscopic structure and the perturbations to this response introduced by both the macroscopic aggregation of leaves in a canopy and the intervening atmosphere is required. This physical problem may be succinctly posed as a radiative transfer equation, the solution of which convolved with an instrument's response function is the remote spectral measurement.

In this paper, the state-of-the-art on modeling of radiation transport in vegetation canopies and the application of such models to the interpretation and analysis of remotely sensed optical data is summarized. We begin with a statement of the physical problem and its mathematical description, parameterization and numerical solution (section II). This is followed by a brief catalogue of the various distortionary effects inherent in remote observations (section III). The extraction of information (namely estimation of vegetation properties) from remote optical measurements is discussed in the last section. This paper is not intended to be a review either of literature or of the various ideas currently in vogue. Instead, it is aimed with the broader scope of itemizing and elaborating three issues in the optical remote sensing of vegetation—modeling, caveats, and algorithms.

II. THE PHYSICAL PROBLEM

In this section we begin with a brief statement of the physical problem encountered in the optical remote sensing of vegetated land surfaces. Forward modeling of the physical problem is developed as boundary value problems in radiative transfer. The parameterization and solution of the resulting equations are discussed along with results of validation of the models.

Statement of the Physical Problem

The atmosphere is illuminated at the top by monodirectional solar radiation that is absorbed and/or scattered depending on the composition of the atmosphere and wavelength of the incident beam. The vegetation canopy

[*]Biospheric Sciences Branch, NASA—Goddard Space Flight Center, Greenbelt, MD
[**]Université Blaise Pascal, Laboratoire de Météorologie Physique, Aubière, France
[†]Department of Aerospace Engineering Studies, University of Colorado, Boulder
[††]Institute for Remote Sensing Applications, CEC Joint Research Center, Ispra (VA), Italy
Address correspondence to R. B. Myneni, Goddard Space Flight Center, Code 923, Greenbelt, MD 20771. R. B. Myneni is a University of Maryland Association Resident Associate.
Received 2 August 1993; accepted 8 August 1994.

REMOTE SENS. ENVIRON. 51:169–188 (1995)

655 Avenue of the Americas, New York, NY 10010
0034-4257/95/$9.50
SSDI 0034-4257(94)00073-V

receives both monodirectional and diffuse radiation (due to collisions in the atmosphere), which it reflects back into the atmosphere according to its bidirectional reflectance distribution function. The remote measurements are typically the angular and spectral distributions of radiations exiting the atmosphere. This physical problem may be succinctly posed as a radiative transfer equation that describes the interaction of photons in the atmosphere-vegetation-soil medium, the solution of which is the remote spectral measurement. In some instances, the spectral radiance field immediately above the canopy is measured. The corresponding radiative transfer problem is also outlined in the following sections.

Forward Problem Formulation

We consider the problem of sensing a vegetated land surface through an atmosphere and are concerned primarily with top-of-the-atmosphere (TOA) spectral radiance fields. We shall denote this as the remote sensing problem, as opposed to the vegetation canopy problem where both direct sunlight and diffuse skylight are incident and top-of-the-canopy spectral radiance fields are of interest.

Remote Sensing Problem

The radiance distribution measured by a sensor of uniform spectral response function aboard a satellite can be simulated as the solution of the following radiative transfer problem. For illustrative purposes, the atmosphere is assumed to be horizontally homogeneous, of finite optical depth τ_A, illuminated spatially uniformly on top ($\tau = 0$) by monodirectional solar radiation of intensity I_o incident along $\underline{\Omega}_o$ ($\mu_o < 0$), and bound at the bottom ($\tau = \tau_A$) by a horizontally heterogeneous vegetation canopy. In the absence of polarization, frequency shifting interactions and emission, which we assume throughout this presentation, the steady state monochromatic radiance or intensity distribution function $I(\tau,\vec{p},\underline{\Omega})$ is given by the boundary value problem

$$(\underline{\Omega}\bullet\vec{\nabla}_\tau + 1)I(\tau,\vec{p},\underline{\Omega}) = \frac{\omega_A}{4\pi}\int_{4\pi} d\underline{\Omega}' P_A(\underline{\Omega}'\bullet\underline{\Omega})I(\tau,\vec{p},\underline{\Omega}'), \quad (1a)$$

$$I(0,\underline{\Omega}) = I_o\delta(\underline{\Omega} - \underline{\Omega}_o), \qquad \mu < 0, \quad (1b)$$

$$I(\tau_A,\vec{p},\underline{\Omega}) = \frac{1}{\pi}\int_{2\pi} d\underline{\Omega}' R_V(\vec{p},\underline{\Omega}' \rightarrow \underline{\Omega})|\mu'|I(\tau_A,\vec{p},\underline{\Omega}'), \quad \mu' < 0, \quad \mu > 0. \quad (1c)$$

Here ω_A is the single scattering albedo, P_A is the rotationally invariant scattering phase function for photon scattering from the direction $\underline{\Omega}'$ into $\underline{\Omega}$ and R_V is the vegetation canopy bidirectional reflectance factor (BRF). The unit vector $\underline{\Omega}(\mu,\varphi)$ has an azimuthal angle φ measured anti-clockwise from the positive x-axis that is directed North, and a polar angle $\theta = \cos^{-1}\mu$ with respect to the outward normal (opposite to the τ-axis, which is directed down into the atmosphere); consequently, $\mu \in (0,1)$ denotes upward directions of photon travel and vice versa. The operator $(\underline{\Omega}\bullet\vec{\nabla}_\tau)$ denotes the directional derivative along $\underline{\Omega}$ in $(\tau,\vec{p})$ space, with $\vec{p} \sim x,y$.

From a numerical point of view it is preferable to separate the uncollided from the collided radiation intensity (Myneni et al., 1990). This we do by letting

$$I(\tau,\vec{p},\underline{\Omega}) \equiv I^o(\tau,\vec{p},\underline{\Omega}) + I^s(\tau,\vec{p},\underline{\Omega}) \quad (2)$$

and substituting in Eq. (1) to result in the following:

(A) *Uncollided Intensity*

$$(\underline{\Omega}\bullet\vec{\nabla}_\tau + 1)I^o(\tau,\vec{p},\underline{\Omega}) = 0, \quad (3a)$$

$$I^o(0,\underline{\Omega}) = I_o\delta(\underline{\Omega} - \underline{\Omega}_o), \qquad \mu < 0, \quad (3b)$$

$$I^o(\tau_A,\vec{p},\underline{\Omega}) = \frac{1}{\pi}\int_{2\pi} d\underline{\Omega}' R_V(\vec{p},\underline{\Omega}' \rightarrow \underline{\Omega})|\mu'|I^o(0,\underline{\Omega}) \times \exp\left[-\frac{\tau_A}{|\mu'|}\right], \quad \mu' < 0, \quad \mu > 0, \quad (3c)$$

the solution of which is

$$I^o(\tau,\underline{\Omega}) = I^o(0,\underline{\Omega})\exp\left[-\frac{\tau}{|\mu|}\right], \qquad \mu < 0, \quad (4a)$$

$$I^o(\tau,\vec{p},\underline{\Omega}) = I^o(\tau_A,\vec{p},\underline{\Omega})\exp\left[-\frac{(\tau_A - \tau)}{|\mu|}\right], \qquad \mu > 0. \quad (4b)$$

(B) *Collided Intensity*

$$(\underline{\Omega}\bullet\vec{\nabla}_\tau + 1)I^s(\tau,\vec{p},\underline{\Omega}) = \frac{\omega_A}{4\pi}\int_{4\pi} d\underline{\Omega}' P_A(\underline{\Omega}'\bullet\underline{\Omega})I^s(\tau,\vec{p},\underline{\Omega}') + \frac{\omega}{4\pi}\int_{4\pi} d\underline{\Omega}' P_A(\underline{\Omega}'\bullet\underline{\Omega})I^o(\tau,\vec{p},\underline{\Omega}') \quad (5a)$$

$$I^s(0,\underline{\Omega}) = 0, \qquad \mu < 0, \quad (5b)$$

$$I^s(\tau_A,\vec{p},\underline{\Omega}) = \frac{1}{\pi}\int_{2\pi} d\underline{\Omega}' R_V(\vec{p},\underline{\Omega}' \rightarrow \underline{\Omega})|\mu'|I^s(\tau_A,\underline{\Omega}'), \quad \mu' < 0, \quad \mu > 0. \quad (5c)$$

Problem (B) can be numerically solved by any of the standard methods in radiative transfer for the collided radiation intensity I^s (for example, by the discrete ordinates method; cf. Myneni et al., 1990). The atmospheric parameters τ_A, ω_A and P_A can be specified for model atmospheres or from measurements (section II, Atmospheric Parameters).

The surface bidirectional reflectance factor R_V that appears in Eqs. (3c) and (5c) is defined as

$$R_V(\vec{p},\underline{\Omega}' \rightarrow \underline{\Omega}) = \frac{\pi I(\tau_A,\vec{p},\underline{\Omega})}{|\mu'|I(\tau_A,\underline{\Omega}')}, \qquad \mu' < 0, \quad \mu > 0, \quad (6)$$

where $I(\tau_A, \underline{\Omega}')$ is the intensity incident on the canopy along $\underline{\Omega}'$ and $I(\tau_A,\vec{p},\underline{\Omega})$ is the surface radiance along $\underline{\Omega}$.

The latter is obtained from a numerical solution of the canopy radiative transfer equation.

The classical approach to modeling radiative transfer in vegetation has been to ignore all plant organs other than leaves, and treat this leaf canopy as a gas with nondimensional planar scattering centers, that is, a turbid medium (Ross, 1981). Such an analogy permits the use of standard theory, with minor modifications to account for the angular orientation of the plane-scatterers. The parameter optical depth depends on the direction of photon travel and the scattering phase functions are not rotationally invariant, thereby precluding the use of polynomial expansion methods for handling the scattering integral (Shultis and Myneni, 1988; Marshak, 1989).

A vegetation canopy may be realistically idealized as aggregations or clumps of leaves distributed randomly in free space (vacuum). The intervening free spaces between the clumps constitute the voids. The voids are convolutely shaped and multiply connected three-dimensional structures broken along those regions where leaves are present. Consequently, a leaf canopy can be abstracted as a binary medium—randomly distributed leaf clumps and voids (Myneni et al., 1991). So, the idea of a continuum host material that is central to radiative transfer is not provided for in leaf canopies at optical wavelengths.

If size of the scatterers is considered in a formulation of the transport problem, it is necessary to include not only the number density of scatterers but also the consequences of introducing finite size gaps (holes or voids) in the medium. Standard transport description based on interaction coefficients derived from elementary volumes is not applicable because of the presence of voids. Moreover, if the far-field assumption is violated, as is the case in a leaf canopy, then the scatterers will cast shadows; hence, information on the spatial distribution of scatterers is required to evaluate cross shadowing (Myneni and Asrar, 1991).

A need for such a theory has a strong basis in experimental observations of exiting radiations measured in opposition to a monodirectional source (Kuusk, 1985). The classical theory assumes an infinite number of uncorrelated nondimensional scatterers thereby affording a continuum description of the configuration space. It is clear that point scatterers cannot cast shadows and thus, the classical theory fails to predict or duplicate experimental observations of exiting radiations, especially about the opposition direction. The theory of photon movement and interactions in media where the scattering centers are finite dimensional-oriented plates, spatially distributed in clumps, with large intervening free spaces has been developed in a series of recent works (Myneni et al., 1991; Myneni and Asrar, 1991; Myneni and Ganapol, 1991; Knyazikhin et al., 1992).

A numerical solution of the transport problem including scatterer size effects has not yet been attempted because of the difficulty of parameterization and complexity of the equation set. Methods based on the exchange of radiosity between finite dimensional scatterers provide an alternative to the study of this difficult problem (Borel et al., 1991; Goel et al., 1991). For remote sensing purposes, where the emphasis is on physically realistic but simple models, heuristic formulations generally suffice (Kuusk, 1985; Jupp et al., 1986; among several others). Of these, the analysis of Verstraete et al. (1990) is especially notable for a precise geometric formultion of the scatterer size effects. One advantageous strategy is to include scatterer size effects in first scattering and resort to classical (point scatterer) theory for multiple scatterings (Marshak, 1989), as described below.

A horizontally heterogeneous vegetation canopy of physical depth Z_C bounded by a flat and anisotropically reflecting soil surface is considered. Specifically, we seek a numerical solution to the following boundary value problem:

$$[\underline{\Omega}\bullet\vec{\nabla} + \sigma(\vec{r},\underline{\Omega})]I(\vec{r},\underline{\Omega}) = \int_{4\pi} d\underline{\Omega}'\sigma_s(\vec{r},\underline{\Omega}'\rightarrow\underline{\Omega})I(\vec{r},\underline{\Omega}') \qquad (7a)$$

$$I(0,\underline{\Omega}) = \frac{1}{|\mu|\pi}\delta(\underline{\Omega}-\underline{\Omega}_o), \qquad \mu<0, \qquad (7b)$$

$$I(Z_C,\vec{p},\underline{\Omega}) = \frac{1}{\pi}\int_{2\pi} d\underline{\Omega}'R_S(\vec{p},\underline{\Omega}'\rightarrow\underline{\Omega})|\mu'| \times I(Z_C,\vec{p},\underline{\Omega}'), \qquad \mu'<0, \qquad \mu>0. \qquad (7c)$$

The above assumes a spatially uniform incidence of unit flux at the top of the canopy ($z=0$), and that R_S is the soil BRF distribution. For convenience we have retained the same geometry as earlier [Eq. (1)] but with the z-coordinate replacing the τ-coordinate, and $\vec{r}\sim(x,y,z)$. Here, σ is the extinction coefficient and σ_s is the differential scattering coefficient that depends on the absolute directions of photon travel $\underline{\Omega}'$ and $\underline{\Omega}$. The rotationally invariant problem is recovered if the slope distribution of scattering centers is random.

Extinction of radiation in a canopy depends on the leaf area density distribution and leaf normal orientation, that is, the slope distribution. It is independent of wavelength. A probabilistic description of the scattering event requires information on the leaf-scattering physics in addition to the above two structural parameters. Simple models of the leaf-scattering phase function describing specular reflection at the leaf surface and diffuse scattering in the leaf interior are available in the literature (Marshak, 1989).

A model for the extinction coefficient that correlates interaction rates between incident and once-scattered photons is used here to describe the hot-spot effect (Stewart, 1990)

$$\tilde{\sigma}(\vec{r},\underline{\Omega},\underline{\Omega}') = \begin{cases} \sigma(\vec{r},\underline{\Omega})\{1-\exp[-\varepsilon D(\underline{\Omega},\underline{\Omega}')]\}, & \text{if } (\underline{\Omega}\bullet\underline{\Omega}')<0, \\ \sigma(\vec{r},\underline{\Omega}), & \text{if } (\underline{\Omega}\bullet\underline{\Omega}')>0, \end{cases} \quad (8)$$

where ε is an empirical parameter related to the ratio of vegetation height to characteristic leaf dimension. Its value was estimated to be between 1 and 8 based on several sets of experimental data (Stewart, 1990). The correlation distance D is

$$D(\underline{\Omega},\underline{\Omega}') = \left[\frac{1}{\mu'^2}+\frac{1}{\mu^2}+\frac{2(\underline{\Omega}'\bullet\underline{\Omega})}{|\mu'\mu|}\right]^{0.5}.$$

This particular model for the modified extinction coefficient has two desirable features, namely, that for $\underline{\Omega} = -\underline{\Omega}'$, $\tilde{\sigma}$ vanishes to result in the hot-spot effect, and for large scattering angles it approaches the standard coefficient σ. Moreover, it is always positive unlike the model proposed by Marshak (1989). The inclusion of $\tilde{\sigma}$ in the transfer problem [Eq. (7)] is discussed below.

As in the previous case, let

$$I(\vec{r},\underline{\Omega}) \equiv I^{\circ}(\vec{r},\underline{\Omega}) + I^{\uparrow}(\vec{r},\underline{\Omega}) + I^{\downarrow}(\vec{r},\underline{\Omega}) + I^{M}(\vec{r},\underline{\Omega}) \quad (9)$$

where I° is the uncollided intensity, I^{1} is the once-collided intensity due to downward incident radiation, and I^{M} is the remainder intensity. Inserting Eq. (9) into Eq. (7) results in the following:

(C) *Downward Uncollided Intensity*

$$[\underline{\Omega}\bullet\vec{\nabla}+\sigma(\vec{r},\underline{\Omega})]I^{\circ}(\vec{r},\underline{\Omega}) = 0, \qquad \mu<0, \quad (10a)$$

$$I^{\circ}(0,\underline{\Omega}) = \frac{1}{|\mu|\pi}\delta(\underline{\Omega}-\underline{\Omega}_o), \qquad \mu<0, \quad (10b)$$

$$I^{\circ}(\vec{r},\underline{\Omega}_o) = \frac{1}{|\mu_o|\pi}\exp\left[-\frac{1}{|\mu_o|}\int_o^{|\vec{r}-\vec{r}_o|} ds'\sigma(\vec{r}-s'\underline{\Omega}_o,\underline{\Omega}_o)\right], \qquad \mu_o<0. \quad (10c)$$

(D) *Upward Uncollided Intensity*

$$[\underline{\Omega}\bullet\vec{\nabla}+\tilde{\sigma}(\vec{r},\underline{\Omega},\underline{\Omega}')]I^{\circ}(\vec{r},\underline{\Omega}) = 0, \qquad \mu>0, \quad (11a)$$

$$I^{\circ}(Z_C,\vec{p},\underline{\Omega}) = \frac{1}{\pi}R_S(\vec{p},\underline{\Omega}_o\rightarrow\underline{\Omega})|\mu_o|I^{\circ}(Z_C,\vec{p},\underline{\Omega}_o), \qquad \mu>0, \qquad \mu_o<0, \quad (11b)$$

$$I^{\circ}(\vec{r},\underline{\Omega}) = I^{\circ}(Z_C,\vec{p},\underline{\Omega})\exp\left[-\frac{1}{|\mu|}\int_0^{|\vec{r}-\vec{r}_C|} ds'\tilde{\sigma}(\vec{r}-s'\underline{\Omega},\underline{\Omega},\underline{\Omega}_o)\right], \qquad \mu>0. \quad (11c)$$

(E) *Downward Once-Collided Intensity due to* I°

$$[\underline{\Omega}\bullet\vec{\nabla}+\sigma(\vec{r},\underline{\Omega})]I^{\downarrow}(\vec{r},\underline{\Omega}) = \sigma_s(\vec{r},\underline{\Omega}_o\rightarrow\underline{\Omega})I^{\circ}(\vec{r},\underline{\Omega}_o), \qquad \mu<0, \qquad \mu_o<0, \quad (12a)$$

$$I^{\downarrow}(0,\underline{\Omega}) = 0, \qquad \mu<0, \quad (12b)$$

$$I^{\downarrow}(\vec{r},\underline{\Omega}) = \int_o^{|\vec{r}-\vec{r}_o|} ds'\exp\left[-\frac{1}{|\mu|}\int_o^{|\vec{r}-\vec{r}'|} ds''\sigma(\vec{r}-s''\underline{\Omega},\underline{\Omega})\right] \times \sigma_s(\vec{r}',\underline{\Omega}_o\rightarrow\underline{\Omega}')I^{\circ}(\vec{r}',\underline{\Omega}_o), \qquad \mu<0, \qquad \mu_o<0. \quad (12c)$$

(F) *Upward Once-Collided Intensity due to* I°

$$[\underline{\Omega}\bullet\vec{\nabla}+\tilde{\sigma}(\vec{r},\underline{\Omega},\underline{\Omega}')]I^{\uparrow}(\vec{r},\underline{\Omega}) = \sigma_s(\vec{r},\underline{\Omega}_o\rightarrow\underline{\Omega})I^{\circ}(\vec{r},\underline{\Omega}_o), \qquad \mu>0, \qquad \mu_o<0, \quad (13a)$$

$$I^{\uparrow}(Z_C,\vec{p},\underline{\Omega}) = 0, \qquad \mu>0, \quad (13b)$$

$$I^{\uparrow}(\vec{r},\underline{\Omega}) = \int_o^{|\vec{r}-\vec{r}_C|} ds'\exp\left[-\frac{1}{|\mu|}\int_0^{|\vec{r}-\vec{r}'|} ds''\tilde{\sigma}(\vec{r}-s''\underline{\Omega},\underline{\Omega},\underline{\Omega}_o)\right] \times \sigma_s(\vec{r}',\underline{\Omega}_o\rightarrow\underline{\Omega})I^{\circ}(\vec{r}',\underline{\Omega}_o), \qquad \mu>0, \qquad \mu_o<0. \quad (13c)$$

(G) *Remainder Intensity* I^{M}

$$[\underline{\Omega}\bullet\vec{\nabla}+\sigma(\vec{r},\underline{\Omega})]I^{M}(\vec{r},\underline{\Omega}) = \int_{4\pi} d\underline{\Omega}'\sigma_s(\vec{r},\underline{\Omega}'\rightarrow\underline{\Omega})I^{M}(\vec{r},\underline{\Omega}') + \int_{4\pi} d\underline{\Omega}'\sigma_s(\vec{r},\underline{\Omega}'\rightarrow\underline{\Omega})I^{1}(\vec{r},\underline{\Omega}') + \int_{2\pi} d\underline{\Omega}'\sigma_s(\vec{r};\underline{\Omega}'\rightarrow\underline{\Omega})I^{\circ}(\vec{r},\underline{\Omega}'), \quad (14a)$$

$$I^{M}(0,\underline{\Omega}) = 0, \qquad \mu<0, \quad (14b)$$

$$I^{M}(Z_C,\vec{p},\underline{\Omega}) = \frac{1}{\pi}\int_{2\pi} d\underline{\Omega}'R_S(\vec{p},\underline{\Omega}'\rightarrow\underline{\Omega})|\mu'|I^{M}(Z_C,\vec{r},\underline{\Omega}') + \frac{1}{\pi}\int_{2\pi} d\underline{\Omega}'R_S(\vec{p},\underline{\Omega}'\rightarrow\underline{\Omega})|\mu'|I^{1}(Z_C,\vec{p},\underline{\Omega}'), \qquad \mu'<0, \qquad \mu>0. \quad (14c)$$

In the above, $\vec{r}_o \sim (0,x,y)$ is a point on the upper surface of the canopy and likewise $\vec{r}_C \sim (Z_C,x,y)$ on the lower (soil) surface. The variable s denotes distance back along the direction $\underline{\Omega}$ such as $\vec{r}' = \vec{r} - s\underline{\Omega}$. It is convenient from a numerical point of view to solve problems (E) and (F) using the discrete ordinates method rather than numerically evaluating Eqs. (12c) and (13c) because the intensity I^{1} is required to specify the source term [Eq. (14a)] and boundary condition [Eq. (14c)] in problem (G). The transfer problems defined by Eqs. (5), (12), (13) and (14) can all be solved by the standard discrete ordinates method (Myneni et al., 1990) or by iterative methods (Knyazikhin and Marshak, 1991) with some minor modifications.

Vegetation Canopy Problem

The canopy radiative transfer problem differs from Eq. (7) in that both direct sunlight and diffuse (collided in the atmosphere) skylight are incident on the canopy.

The atmospheric radiative transfer problem [Eq. (1)] must be solved first in order to specify the boundary conditions for the canopy problem. In this section, a brief description of the canopy problem is given.

The governing radiative transfer equation and boundary conditions are of the form

$$[\underline{\Omega}\cdot\vec{\nabla}+\sigma(\vec{r},\underline{\Omega})]I(\vec{r},\underline{\Omega})=\int_{4\pi}d\underline{\Omega}'\sigma_s(\vec{r},\underline{\Omega}'\rightarrow\underline{\Omega})I(\vec{r},\underline{\Omega}') \quad (15a)$$

$$I(0,\vec{p},\underline{\Omega})=I_E\exp\left[-\frac{\tau_A}{|\mu|}\right]\delta(\underline{\Omega}-\underline{\Omega}_o)+I_d(0,\vec{p},\underline{\Omega}),\qquad \mu<0, \quad (15b)$$

$$I(Z_C,\vec{p},\underline{\Omega})=\frac{1}{\pi}\int_{2\pi}d\underline{\Omega}'R_S(\vec{p},\underline{\Omega}'\rightarrow\underline{\Omega})|\mu'|\times I(Z_C,\vec{p},\underline{\Omega}'),\qquad \mu'<0,\ \mu>0, \quad (15c)$$

where I_E is the extra-terrestrial solar radiation incident at the top of the atmosphere along $\underline{\Omega}_o$ about wavelength λ. The term $I_d(0,\vec{p},\underline{\Omega})$ is the atmospheric intensity distribution incident on the canopy and is obtained from a numerical solution of the transfer problem denoted by Eq. (5), that is, the atmospheric transmittance. The atmospheric transmittance can be spatially averaged without loss of much accuracy. With this simplification, the canopy radiative transfer problem [Eq. (15)] can be reduced to the following problems [cf. Eq. (9)]:

(H) *Downward Uncollided Intensity*

$$[\underline{\Omega}\cdot\vec{\nabla}+\sigma(\vec{r},\underline{\Omega})]I_\downarrow^c(\vec{r},\underline{\Omega})=0,\qquad \mu<0, \quad (16a)$$

$$I_\downarrow^c(0,\underline{\Omega})=I_E\exp\left[-\frac{\tau_A}{|\mu|}\right]\delta(\underline{\Omega}-\underline{\Omega}_o)+I_d(0,\underline{\Omega}),\qquad \mu<0, \quad (16b)$$

$$I_\downarrow^c(\vec{r},\underline{\Omega})=I_\downarrow^c(0,\underline{\Omega})\times\exp\left[-\frac{1}{|\mu|}\int^{|\vec{r}-\vec{r}_o|}ds'\sigma(\vec{r}-s'\,\underline{\Omega},\underline{\Omega})\right],\qquad \mu<0. \quad (16c)$$

(I) *Upward Uncollided Intensity*

$$[\underline{\Omega}\cdot\vec{\nabla}+\tilde{\sigma}(\vec{r},\underline{\Omega},\underline{\Omega}_i)]I_{\uparrow i}^c(\vec{r},\underline{\Omega})=0,\qquad \mu>0, \quad (17a)$$

$$I_{\uparrow i}^c(Z_C,\vec{p},\underline{\Omega})=\frac{1}{\pi}R_S(\vec{p},\underline{\Omega}_i\rightarrow\underline{\Omega})|\mu_i|I_\downarrow^c(Z_C,\vec{p},\underline{\Omega}_i),\qquad \mu>0,\ \mu_i<0, \quad (17b)$$

$$I_{\uparrow i}^c(\vec{r},\underline{\Omega})=I_{\uparrow i}^c(Z_C,\vec{p},\underline{\Omega})\exp\left[-\frac{1}{|\mu|}\int_0^{|\vec{r}-\vec{r}_C|}ds'\tilde{\sigma}(\vec{r}-s'\underline{\Omega},\underline{\Omega},\underline{\Omega}_i)\right],\qquad \mu>0. \quad (17c)$$

$$I_\uparrow^c(\vec{r},\underline{\Omega})=\sum_i I_{\uparrow i}^c(\vec{r},\underline{\Omega}),\qquad i=0,1,\ldots,N$$

(J) *Downward Once-Collided Intensity due to* $I_\downarrow^c$

$$[\underline{\Omega}\cdot\vec{\nabla}+\sigma(\vec{r},\underline{\Omega})]I_\downarrow^1(\vec{r},\underline{\Omega})=\int_{2\pi}d\underline{\Omega}'\sigma_s(\vec{r},\underline{\Omega}'\rightarrow\underline{\Omega})I_\downarrow^c(\vec{r},\underline{\Omega}'),\qquad \mu<0,\ \mu_o<0, \quad (18a)$$

$$I_\downarrow^1(0,\underline{\Omega})=0,\qquad \mu<0, \quad (18b)$$

$$I_\downarrow^1(\vec{r},\underline{\Omega})=\int_o^{|\vec{r}-\vec{r}_o|}ds'\exp\left[-\frac{1}{|\mu|}\int_0^{|\vec{r}-\vec{r}'|}ds''\sigma(\vec{r}-s''\underline{\Omega},\underline{\Omega})\right]\times\int_{2\pi}d\underline{\Omega}'\sigma_s(\vec{r}',\underline{\Omega}'\rightarrow\underline{\Omega})I_\downarrow^c(\vec{r},\underline{\Omega}'),\qquad \mu<0,\ \mu_o<0. \quad (18c)$$

(K) *Upward Once-Collided Intensity due to* $I_\downarrow^c$

$$[\underline{\Omega}\cdot\vec{\nabla}+\tilde{\sigma}(\vec{r},\underline{\Omega},\underline{\Omega}_i)]I_{\uparrow i}^1(\vec{r},\underline{\Omega})=\sigma_s(\vec{r},\underline{\Omega}_i\rightarrow\underline{\Omega})I_\downarrow^c(\vec{r},\underline{\Omega}_i),\qquad \mu>0,\ \mu_i<0, \quad (19a)$$

$$I_{\uparrow i}^1(Z_C,\vec{p},\underline{\Omega})=0,\qquad \mu>0, \quad (19b)$$

$$I_{\uparrow i}^1(\vec{r},\underline{\Omega})=\int_o^{|\vec{r}-\vec{r}_C|}ds'\exp\left[-\frac{1}{|\mu|}\int_0^{|\vec{r}-\vec{r}'|}ds''\tilde{\sigma}(\vec{r}-s''\underline{\Omega},\underline{\Omega},\underline{\Omega}_i)\right]\times\sigma_s(\vec{r},\underline{\Omega}_i\rightarrow\underline{\Omega})I_\downarrow^c(\vec{r}',\underline{\Omega}_i),\qquad \mu>0,\ \mu_i<0. \quad (19c)$$

$$I_\uparrow^1(\vec{r},\underline{\Omega})=\sum_i I_{\uparrow i}^1(\vec{r},\underline{\Omega}),\qquad i=0,1,\ldots,N$$

(L) *Remainder Intensity* I^M

Same as Problem (G)—Eq. (14)

In the above equations, I_d is the spatially averaged atmospheric transmittance incident along $\underline{\Omega}_i$ with $i=0,1,2,\ldots,M$, where $2M$ is the number of discrete directions in the unit sphere. The index $i=0$ corresponds to the incident solar direction $\underline{\Omega}_o$ with the assumption that $\underline{\Omega}_o\notin Q_N$, where Q_N is the quadrature set of discrete ordinates. A particular advantage of this formulation is that it circumvents the ambiguity associated with the coefficient $\tilde{\sigma}$, which has a dependence on the photon's previous direction of travel [namely Eqs. (17) and (19)].

Parameterization, Solution, and Validation

In the section entitled "Forward Problem Formulation" we have seen how the forward modeling of the physical problem can be posed as boundary value problems in radiative transfer. A numerical solution of these equations requires parameterization of the composition and optical properties of the media in question. This issue is addressed here together with some examples of model validation.

Atmospheric Parameters

Atmospheric optical depth τ_A, single scattering albedo ω_A and phase function P_A are parameterized for standard, cloudless, and horizontally homogeneous atmo-

spheres. Molecular optical depth τ_λ^m at wavelength λ is evaluated from refractive index of air and molecular density distribution. Routines from the 5S code can be used to calculate τ_λ^m and the Rayleigh phase function P^m (Tanré et al., 1990). The profile of the atmospheric aerosol distribution is based on a recommendation by the International Radiation Commission (IRC) applicable to continental areas with an aerosol optical depth of 0.23 at 0.55 μm (Deepak and Gerber, 1983). The aerosol scattering phase function P^a can be modeled using the Henyey–Greenstein function or other such analytical expressions. The asymmetry parameter of the Henyey–Greenstein function g^a and the aerosol single scattering albedo ω^a are tabulated in the IRC report for several wavelengths in the solar spectrum. The total atmospheric optical depth τ_A, single scattering albedo ω_A and the scattering phase function P_A are evaluated assuming external mixing. A modified version of LOWTRAN-7 is used to select wavelength bands where atmospheric absorption is less than 0.1 (S. C. Tsay, personal communication). Both line and continuum absorption by 16 gaseous species at any solar zenith angle can be considered in selecting these windows (Table 1).

Canopy Parameters

Numerical evaluation of the coefficients σ and σ_s in Eqs. (7a) and (15a) requires information on the leaf-area density distribution in the stand u_L, leaf normal orientation distribution g_L and the leaf scattering phase function γ_L. A vegetation canopy can be simulated as clumps of leaves randomly distributed on a reflective soil with a ground cover (g_c) between 0 and 100%. A flat horizontal ground area (a_s) of dimensions $X_S \times Y_S$ is considered for simulation purposes. The height of the canopy is assumed equal to the height of the clumps ($Z_S = Z_C$). If L_c is the clump leaf-area index, then by definition, the canopy leaf area index is given by the product $g_c \times L_c$. Leaf-area density distribution inside the clumps can be modeled using simple analytical functions, namely quadratic (Myneni et al., 1990). For instance, if leaf area inside a clump is assumed to be uniformly distributed, then $u_L = L_c / Z_C$.

The leaf normal orientation can be assumed to be azimuthally symmetric. The distribution along the polar angle can be modeled using the standard distributions: planophile, erectophile, plagiophile, extremophile, and uniform. The discrete Beta distribution is recommended because of its simplicity and versatility (Strebel et al., 1985). With only two parameters this distribution represents most leaf normal orientations encountered in nature.

The leaf scattering phase function γ_L, can be written as the sum of diffuse scattering inside the leaf (γ_{LD}) (the bi-Lambertian model; Ross, 1981) and specular reflection at the leaf surface (γ_{LS}) (Vanderbilt and Grant, 1985). The leaf spectral reflectance (r_L) and transmittance (t_L) are typically measured with integrating spheres. They can also be simulated using models of radiation transport in leaves. Jacquemoud and Baret (1990) developed one such model that allows simulation of r_L and t_L in the 0.4–2.5 μm interval, using only three parameters—a parameter characterizing leaf mesophyll structure, chlorophyll concentration, and leaf water content. Table 2 presents values of standard leaf optical properties for the wavelength bands of interest.

Soil Parameters

Bidirectional reflectance factors of the soil, R_S, can be described following Hapke's formulation applied to bare rough soil surfaces (Pinty et al., 1989; Jacquemoud et al., 1992). The soil is assumed to be a half-space (semi-infinite) and first-collision intensity is evaluated analytically, with shadows included to model the hot spot effect. Multiple scattering is simplified to a two-stream problem. Standard values for the coefficients (b, c, b', c') of the Legendre polynomial expansion for the particle phase function, and the parameter h related to the porosity of the medium, are given in Jacquemoud et al. (1992). The single scattering albedo of the soil particu-

Table 1. Atmospheric Parameters Used in the Base Case

Atmospheric parameters					
Wavelength (micrometers)	*Incident energy (w/ms)*	*Rayleigh optical depth*	*Aerosol optical depth*	*Aerosol single scat. albedo*	*Anisotropic parameter*
0.4011–0.5133	214.48	0.200	0.282	0.899	0.642
0.5153–0.5333	37.00	0.114	0.242	0.896	0.638
0.5353–0.5873	102.15	0.086	0.225	0.892	0.637
0.5893–0.6852	163.57	0.051	0.194	0.887	0.633
0.6912–0.6972	14.49	0.036	0.175	0.880	0.631
0.8280–0.8940	69.62	0.015	0.132	0.842	0.632

Within these wavelength bands atmospheric absorption is less than 10%. A clear and turbid atmospheric conditions were simulated by doubling and halving the total atmospheric optical depth in each waveband.

Table 2. Canopy and Soil Parameters Used in the Base Case

Canopy and soil parameters					
Wavelength (μm)	*Leaf hemispherical reflectance*	*Leaf hemispherical transmittance*	*Single scattering albedo of soil particulates*		
			Sand	*Clay*	*Peat*
0.4011–0.5133	0.058	0.008	0.470	0.217	0.061
0.5153–0.5333	0.108	0.061	0.445	0.198	0.045
0.5353–0.5873	0.131	0.084	0.536	0.214	0.054
0.5893–0.6852	0.083	0.038	0.600	0.267	0.074
0.6912–0.6972	0.091	0.051	0.612	0.271	0.081
0.8280–0.8940	0.510	0.418	0.710	0.316	0.194

The leaf optical properties are average values of several measured spectra (F.G. Hall, Personal communication). The soil values are taken from Jacquemoud et al. (1992).

lates ω_S is the only parameter dependent on wavelength and soil moisture (Fig. 4 in Jacquemoud et al., 1992), although this assumption is not necessarily beyond debate. The single scattering albedo of clay, sand, and peat particulates, integrated over the wavebands of interest, are given in Table 2.

Numerical Solution

The radiative transfer problems [Eqs. (1) and (15)] can be simplified and approximated under a variety of assumptions. The medium may be assumed to be horizontally homogeneous to permit a one-dimensional analysis. The transport equation can be azimuthally averaged to result in a one-angle problem (Shultis and Myneni, 1988) or integrated over all directions to obtain flux transport equations (Suits, 1972). The medium can be assumed to be semi-infinite to allow substantial simplifications (Verstraete et al., 1990). The leaf-normal orientation can be assumed to be a delta function to facilitate semi-analytical solutions (Ganapol and Myneni, 1992). Multiple scattering can be approximated using solutions of flux propagation equations (Nilson and Kuusk, 1989). Similarly, assumptions about the boundary conditions (vacuum and/or isotropic boundary conditions) facilitate numerical solution of the transport problem (Dickinson et al., 1990). Detailed reviews of literature relevant to optical remote sensing problems can be found elsewhere (Goel, 1988; Kaufman, 1989; Myneni and Ross, 1991).

The standard discrete ordinates method with some modifications can be employed to numerically solve the transfer problems (B), (E)-(G), (J)-(L), for the radiation intensity $I(\vec{r},\underline{\Omega})$. The discrete ordinates algorithm satisfies photon conservation and guarantees positivity, homogeneity and stability of the solution (Knyazikin and Marshak, 1991).

The angular variable $\underline{\Omega}$ is discretized using equal weight (EQ_N) quadrature sets of order N (or other quadrature schemes), thereby restricting the flight of photons to discrete quadrature ordinate directions. The spatial derivatives are approximated by finite difference schemes (or, finite elements). The resulting algebraic system of equations are solved iteratively on the scattering source by the method of sweeping in the phase-space grid. Convergence of this iteration is slow in optically deep canopies and in situations where the single scattering albedo is close to unity. Hence, it is desirable to accelerate convergence of the iteration, for which several standard methods exist (Myneni et al., 1990).

The calculation scheme is as follows. The canopy BRF matrix R_V is evaluated first [Problems (C)-(G)]. The atmospheric transfer problem is then solved using this matrix [Problems (A)-(B)]. The radiation field incident on the canopy is now known [Eq. (15b)]. So, the canopy transport problem can be solved [Problems (H)-(L)]. A detailed energy balance is performed at each level. Interpolation schemes to decouple quadrature orders between the canopy and atmospheric radiative transfer calculations can be implemented for tailoring accuracy and also to evaluate the radiance field in desired angular grids. Essentially this involves performing one additional sweep of the phase-space, using the converged source distribution, into the desired angular grid. This entire scheme is wavelength specific. Details on the application of the discrete ordinates method for numerical solution of the transport equation can be found in Myneni et al. (1990).

Model Comparison and Results

A comparison of four different models with varying assumptions, but all based on a numerical solution of the transfer equation, is shown in Figure 1a. The implementation of our discrete ordinates method was rigorously benchmarked and found to be four-digit accurate (Myneni et al., 1988; Ganapol and Myneni, 1992). The method was also validated with experimental data of reflectance spectra collected over maize and soybean (Myneni et al., 1988; Shultis and Myneni, 1988; Stewart, 1990; Myneni and Asrar, 1993), prairie grassland (Asrar et al., 1989) and forest canopies (Myneni et al., 1992).

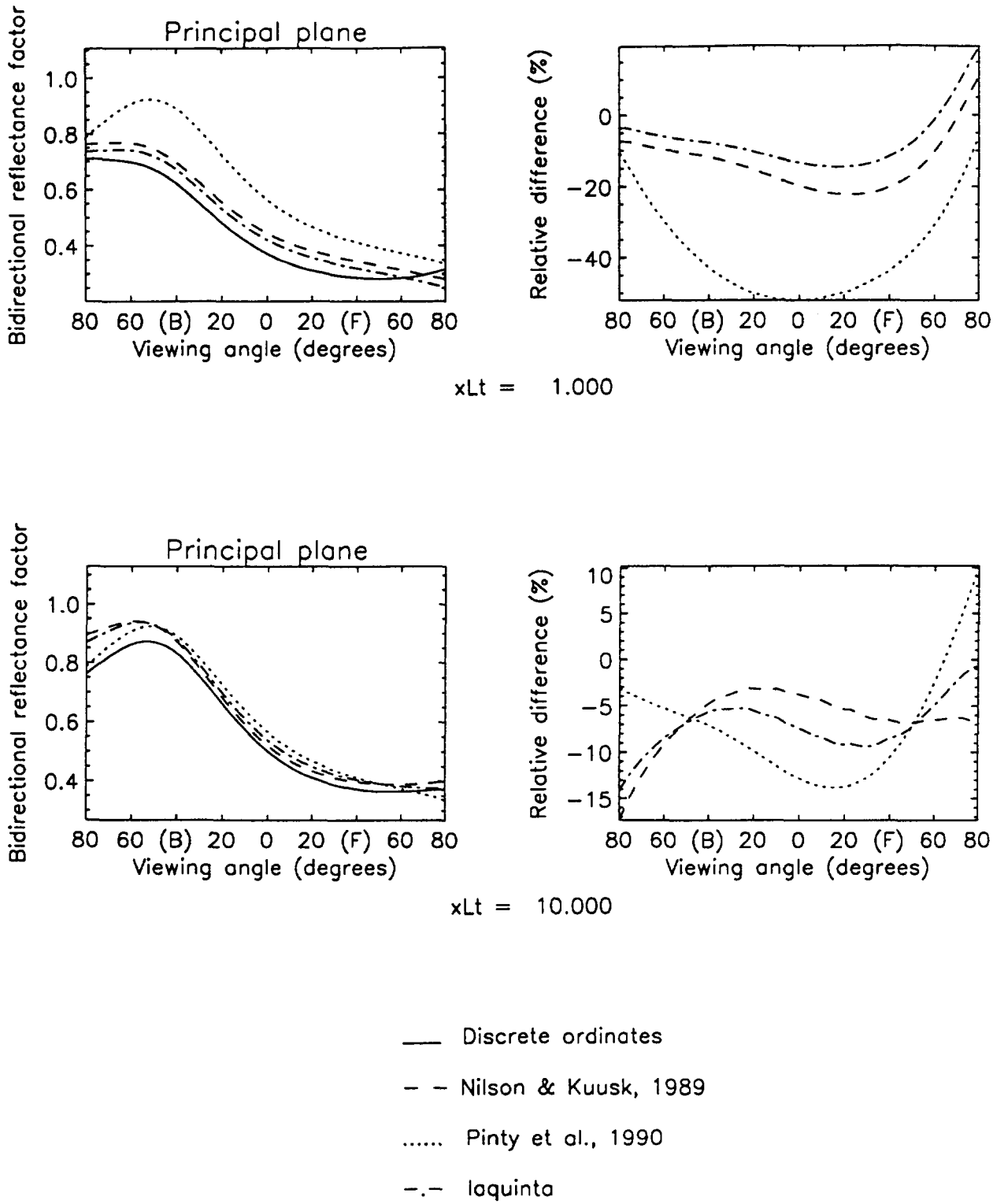

Figure 1a. Comparison of canopy bidirectional reflectance factors in the solar principal plane as predicted by different models. The canopy leaf area index (xLt) is 1 and 10. The leaf normal orientation is erectophile in polar angle and uniform in azimuth. Leaf single scattering albedo is 0.9 and scattering from soil is assumed Lambertian with a hemispherical reflectance value of 0.3. Henyey-Greenstein phase function with a backscattering asymmetry parameter ($g = -0.4$) was used in all the models. The hot spot effect was suppressed in all the models because of different parameterizations. The solar zenith and azimuth angles are 45° and 180°, respectively. The discrete ordinates model is of Shultis and Myneni (1988) and is used here as a reference. The other models are described in Nilson and Kuusk (1989) and Pinty et al. (1990). The model of Iaquinta (unpublished) combines the first scattering of Verstraete et al. (1990) with the two-stream model of Sellers (1985).

The discrete ordinates model will be used as the benchmark. The model of Pinty et al. (1990) is notable for it considers a canopy of infinite thickness. All of the models except the discrete ordinates use a flux approximation for multiple scattering. Of these, it appears that a model based on an accurate evaluation of first scattering and the two-stream model of Sellers (1985) for multiple scattering gives the best approximation to the solution of the transfer equation (the unpublished model of Iaquinta). In general, results of comparison of model predictions with empirical data, although satisfactory in many cases, reveal two major deficiencies in most models; namely, the effects of clumping and size of canopy elements. A realistic treatment of these effects and a simplified three-dimensional model of radiation transfer are topics for future studies.

For vegetation, one generally deals with wavelengths in two spectral regions located on both sides of 0.7 μm. Indeed, the strong chlorophyll absorption that corresponds to low values of the single scattering albedo (less than 0.2) should allow us to retrieve both the optical and structural properties of the medium because of the resulting high anisotropy in the exiting radiance field. The near infrared region is characterized by high leaf reflectance and transmittance, allowing radiation to easily reach the ground after multiple scattering events. Moreover, the exiting radiance field is less anisotropic because photons are diffused in all directions due to multiple collisions. This means that the retrieval of canopy properties will be more difficult. Thus, the ratio of single to total scattering is an indicator of the canopy behaviour with respect to its intrinsic radiative properties (Figure 1b). The ratio is strongly nonlinear with respect to leaf area index and the single scattering albedo. It can be seen that the single scattered radiance is less than 50% of the total radiance for the large part. This clearly indicates that the multiple scattering component has to be modeled rather accurately for extracting quantitative information from data collected over this single scattering albedo-leaf area index domain.

CAVEATS IN REMOTE SENSING

The central hypothesis in remote sensing is that radiation reflected from a surface carries information about the state of the surface. The appropriation of signal characteristics with surface properties is complicated for one can never measure in isolation the desired cause and effect in the system. In the remote sensing of vegetation from satellite-borne instruments, several caveats are in order. Several of these are discussed in this section.

Bidirectional Effects

The angular distribution of top-of-the-canopy (TOC) spectral radiance is shown in Figure 2a for two wavelengths and solar zenith angles. The canopy leaf area index is 3 and uniform leaf normal orientation distribu-

Figure 1b. The ratio of single to total scattered radiance obtained from a two-stream model (Sellers, 1985). The illumination angle is 45°, the soil albedo is 0.3 and the leaf normal orientation is uniform.

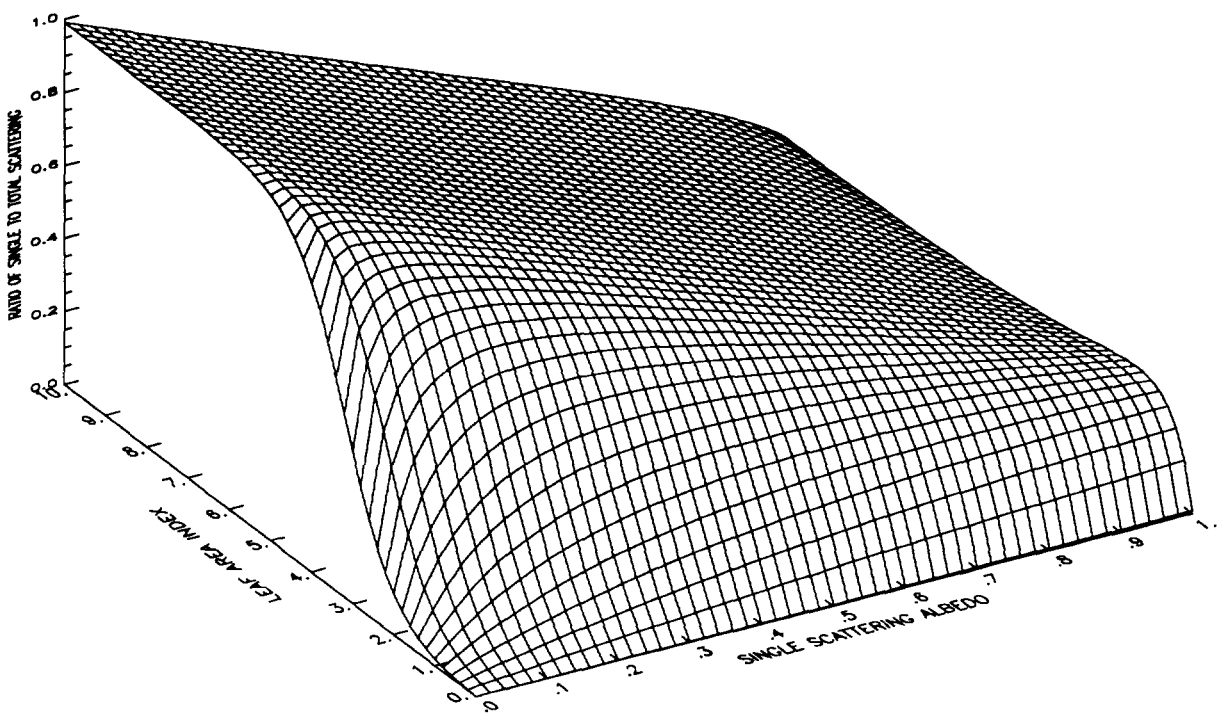

tion is assumed. The other parameter values are given in Tables 1 and 2. At both wavelengths, the distributions are anisotropic with the hot spot in the retro-solar direction. The hot-spot radiance is, in general, the maximum of the distribution. The minimum is found near the nadir on the forward scattering side. The hot-spot effect is more pronounced in the red than near-infrared because of the contrast between sunlit and shaded elements. The degree of anisotropy increases with solar zenith angle. From these results, it can be seen that differences in radiance observations measured at different solar and view angles are not necessarily attributable to changes in the surface. The differences may be due to bidirectional effects of the radiance field.

Atmospheric Effects

The corresponding angular distribution of top-of-the-atmosphere (TOA) spectral radiance field is shown in Figure 2b. TOA radiances differ from those above the canopy both in terms of their magnitude and angular distribution. The net atmospheric effect, which is the difference between TOA and TOC values, decreases almost linearly with increasing surface reflectance (Kaufman, 1989). It is positive at shorter wavelengths (namely red) where atmospheric scattering plays a dominant role and negative at longer wavelengths (near-infrared) where aerosol and gaseous absorption predominate. For instance, TOA radiance at the red wavelength is 2 to 10 times greater than TOC red radiance depending on the view and solar zenith angles. The hot-spot effect so distinctive at this wavelength in the TOC radiance distribution is masked due to scattering in the atmosphere. At near-infrared wavelengths, the net atmospheric effect is only slightly negative. The TOA radiance distribution at this wavelength is similar to that above the canopy. When remote sensing vegetation through an atmosphere, these spectral atmospheric effects must be corrected.

Canopy Structural Effects

The architecture of a leaf canopy, for the purposes of studying radiation transport, can be characterized by the canopy height, leaf size, orientation and density distribution. Leaf size distribution and canopy height determine the amplitude and width of the vegetation hot spot (Marshak, 1989). The influence of leaf orientation on TOC spectra is shown in Figure 3, together with the spectrum of a leaf simulated with the PROSPECT model of Jacquemoud and Baret (1990). If a parameter such as the leaf area index is to be determined

Figure 2a. Angular distribution of top of the canopy radiance in the solar principal plane at red and near-infrared wavelength. Unit incident irradiance is assumed such that radiance $\times \pi$ is the corresponding bidirectional reflectance factor. θ_o is the solar zenith angle in degrees.

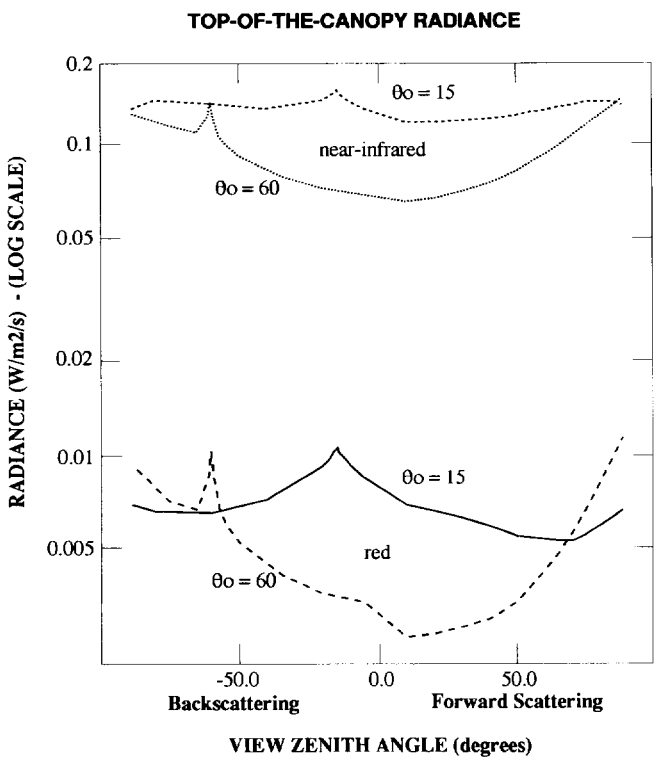

Figure 2b. Angular distribution of top of the atmosphere radiance in the solar principal plane at red and near-infrared wavelength. Unit incident irradiance is assumed such that radiance $\times \pi$ is the corresponding bidirectional reflectance factor. θ_o is the solar zenith angle in degrees.

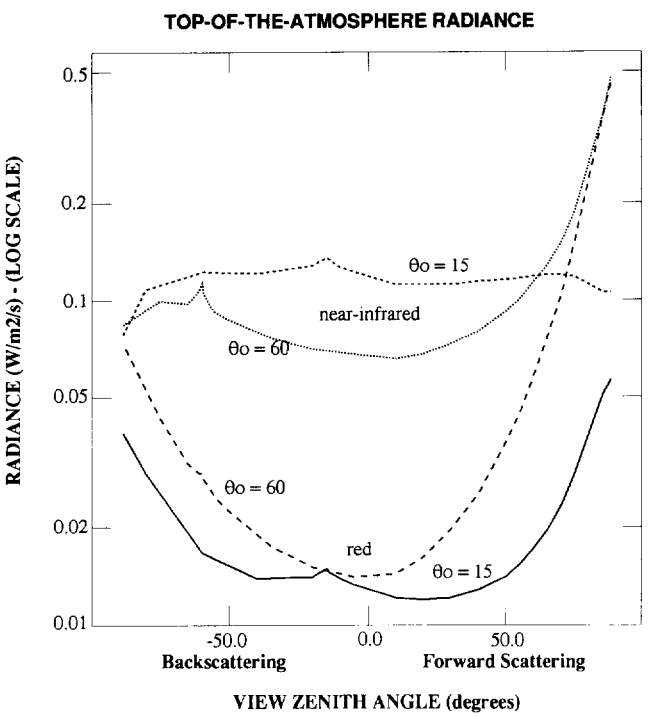

from remote radiance observations, the structural effect due to leaf orientation must be kept in mind.

Background or Soil Effects

The radiance field measured above the vegetated land surface is a composite of both soil and vegetation contributions. When vegetation parameters are to be determined from TOC measurements, methods to minimize the contribution of the soil must be developed (Huete, 1988). On the other hand, when surface parameters such as the albedo are of interest, it is important to accurately include soil contribution. This is illustrated in Figure 4, where surface albedo is plotted against canopy leaf area index for different canopy parameters and for the cases of a bright and a dark soil. Soil brightness determined the nature of the relationship between surface albedo and canopy LAI. When bare soil and dense canopy albedo are comparable in magnitude, as in bright soil simulation (0.27 and 0.30, respectively), surface albedo is a weak function of leaf area index. On the other hand, if the soil is absorptive (bare-soil albedo is 0.06), surface albedo increases near-linearly for LAIs < 3, after which it tends to an asymptote. Hence, the surface albedo of a vegetated land surface can vary widely depending upon soil brightness.

Nonlinear Effects of Scattering

The radiative transfer problem is linear in incident radiation, but nonlinear in scattering. The consequences of non-linearity are illustrated in Figure 5, where the change in TOC nadir bidirectional reflectance factor (BRF) is plotted against the single scattering albedo (sum of leaf reflectance and transmittance) at two values of canopy leaf area index (LAI). In the case of a sparse canopy (LAI = 1), changes in leaf reflectance ($\Delta r_L = 0.05$ & 0.1) at any value of the single scattering albedo are not detectable in TOC nadir BRFs. On the other hand for a dense canopy (LAI = 5), changes in leaf reflectance are detectable in TOC BRFs, which depend non-linearly on the single scattering albedo. These effects are important in the remote sensing of leaf biochemical constituents, where changes in constituent concentration translate into changes in leaf optical properties.

Effects of Spatial Heterogeneity

Spatial distribution of the radiance field and associated processes is affected by spatial heterogeneity of the vegetated surface. Heterogeneity can be conceptually quantified at a macroscopic scale by ground cover and plant spatial distribution. The structural and optical properties of plants in a given area are spatially distributed under natural conditions. As a first approximation, these properties may be assumed spatially invariant; that is, the plants in a given area are identical. In this case, spatial heterogeneity can be prescribed by ground cover, plant spatial distribution, and plant leaf area index. The importance of spatial heterogeneity arises in the context of scaling point observations to areal values.

Figure 3. Spectral distribution of nadir vegetation bidirectional reflectance factors for canopies with different leaf normal orientations. The leaf area index of the canopies is 3. The solar zenith and azimuth angles are 30° and 0°. The corresponding leaf hemispherical reflectance spectrum is also shown.

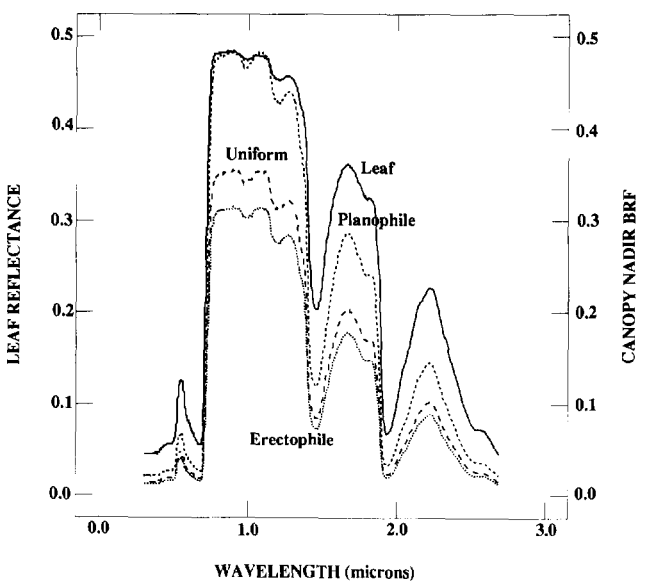

Figure 4. Surface albedo and canopy leaf area index for dark and bright soils, and planophile and erectophile canopies. Leaf hemispherical reflectance and transmittance at visible wavelengths are denoted as r_L and t_L, respectively.

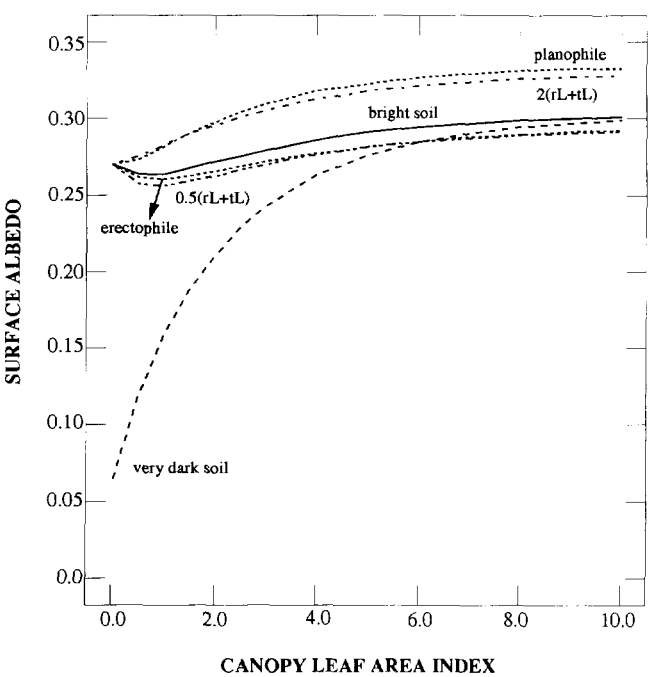

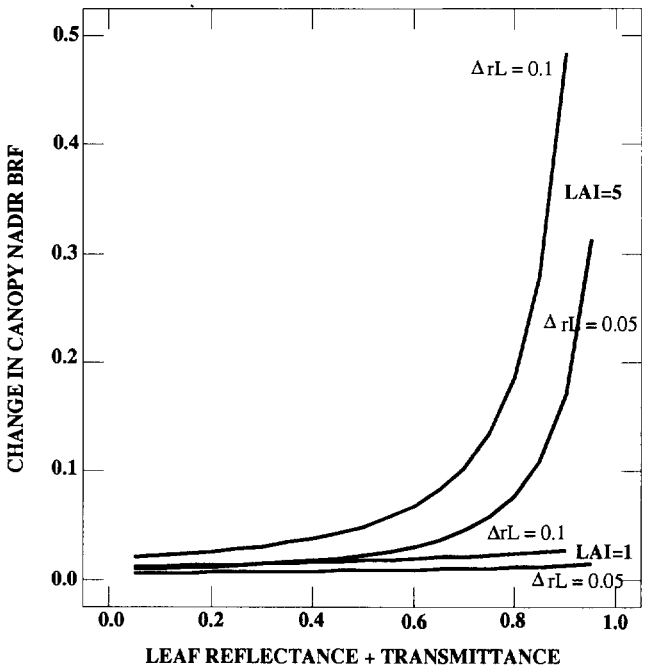

Figure 5. Change in vegetation canopy nadir bidirectional reflectance factor with single scattering albedo (sum of leaf hemispherical reflectance, r_L, and transmittance, t_L).

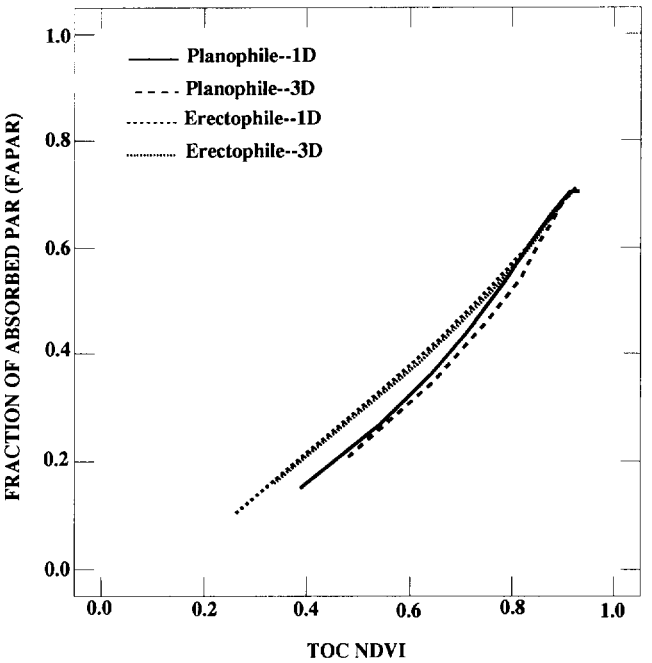

Figure 6. The relationship between the fraction of photosynthetically active radiation absorbed by vegetation (FAPAR) and top-of-the-canopy normalized difference vegetation index (TOC NDVI) in homogeneous (1D) and heterogeneous (3D) canopies with different leaf normal orientation distributions.

The relationship between the fraction of photosynthetically active radiation absorbed by the photosynthesizing tissue in a canopy (FAPAR) and the bidirectional reflectance transform NDVI is an example of scale invariance (Figure 6). It can be seen that the relationship between FAPAR and TOC NDVI is similar for homogeneous (1D) and heterogeneous (3D) canopies. There is a near-unique correspondence between TOC NDVI and FAPAR irrespective of the spatial distribution of leaf area. A given value of TOC NDVI might result from various configuations of ground cover and plant leaf area index. In all such cases, FAPAR is nearly unique. This relationship is scale invariant, for pixels of different spatial scales but of equivalent values of TOC NDVI are likely to have equivalent FAPAR values.

Adjacency Effects

The radiance field measured by a remote sensor may contain contributions from areas adjacent to the target of interest because of scattering in the atmosphere into the field of view. The adjacency effects result in loss of contrast when ground areas of varying reflectivities are observed. This is illustrated in Figure 7, where the square wave modulation transfer function (MTF) is plotted against spatial frequency. The MTF of an optical system describes the variation in output contrast between the peaks and valleys of a sinusoidal or square-wave pattern as a function of spatial frequency (Diner and Martonchik, 1984),

Figure 7. The square-wave normalized modulation transfer function of strip field ground albedo pattern for three atmospheres evaluated from nadir intensities using Eq. 20.

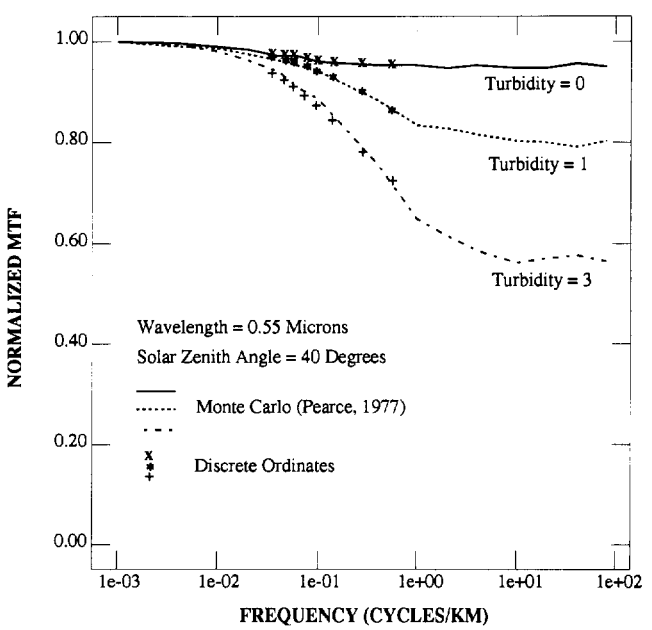

$$\mathrm{MTF}(\Delta X) = \frac{1}{\mathrm{MTF}_\infty}\left[\frac{I(\Delta X/2,y,0,\underline{\Omega}) - I(-\Delta X/2,y,0,\underline{\Omega})}{I(\Delta X/2,y,0,\underline{\Omega}) + I(-\Delta X/2,y,0,\underline{\Omega})}\right] \quad (20)$$

where ΔX is width of the strip, and MTF_∞ is the MTF as $\Delta X \to \infty$. The adjacency effects reduce the contrast between alternating bright and dark strips with increase in atmospheric optical depth and frequency of ground reflectivity variations.

Nonlinear Mixing

The radiance measured by a remote instrument can be written as the sum of component radiances because the governing equation is linear in radiance. For instance, the total radiant intensity can be written as the sum of unscattered, once-scattered, and multiply-scattered radiant intensities. With respect to the problem parameters, such as incident and observation angles, leaf area index (or, optical depth), canopy single scattering albedo and soil reflectance, the equation is nonlinear because of the multiple scattering term. The nonlinear effect due to scattering between leaves and soil is particularly relevant in this context. Consider, for instance, a pixel of incomplete ground cover. The radiance of this pixel is not a linear combination of the vegetation and soil radiances because of the radiative interaction between the vegetation and soil due to multiple scattering. This is illustrated in Figure 8 where the pixel radiance at near-infrared is plotted against the radiance at red. The linear mixing model assumes that vegetation and soil radiances can be combined linearly with weights proportional to ground cover. This assumption is clearly violated under natural conditions because of multiple bounces of photons between leaves and the soil. Thus, care must be excercised when multispectral data are analyzed to derive information on the scene components based on linear mixing models.

Topographic Effects

It has long been recognized that topography can significantly modulate remotely sensed radiances, leading to errors in retrieved surface reflectances. For an unvegetated sloping surface, topography affects the estimation of reflectances from TOA radiances in two ways. First, the amount of energy incident on a surface is a function of topography (via slope, aspect, and shadowing). Second, the upwelling flux off the surface is also dependent on the position of the slope relative to the sensor. Topographic factors that must be considered include elevation, slope, aspect, local shadowing by nearby terrain, obstruction of diffuse sky radiation by nearby terrain, and the configuration of nearby terrain relative to the slope of determining the amount of energy reflected towards the slope. The problem is confounded because topographic effects are dependent on the waveband of interest and on the resolution of the sensor. If the IFOV includes many different terrain elements (resolutions greater than a hundred meters or so) each element has its own topographic effect and contribution to the total radiance. This creates a very difficult inversion problem. A summary of topographic effects and some correction strategies can be found in Dozier (1989) and Dubayah (1992).

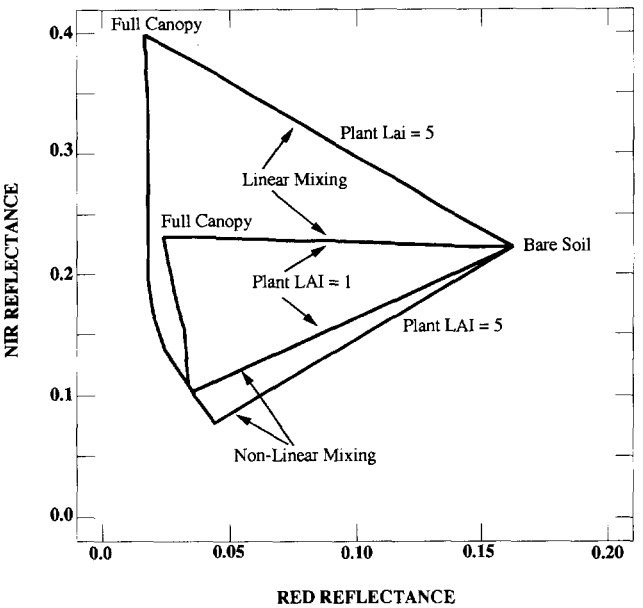

Figure 8. Relationship between canopy nadir bidirectional reflectance factors at red and near-infrared wavelengths. Canopies of varying leaf area indices were simulated by changing ground cover (0–100%) and plant leaf area index (PLAI = 1 & 5). The nonlinear mixing results were obtained from a solution of the three-dimensional radiative transfer equation.

Existing correction models are probably of limited applicability for vegetated surfaces. The elements of a canopy are rarely oriented parallel to a slope; therefore, the effect of the underlying slope is not clear. Research is needed to couple topographic formulations with canopy radiative transfer models. Such a coupled model could be used toward the development of a systematic approach for correcting radiances from vegetated surfaces for topographic effects.

ALGORITHMS

Algorithms in remote sensing are tools that connect radiance measurements to surface properties of interest. In vegetation remote sensing one can make a distinction between radiation model parameters (leaf area index, leaf and soil optical properties, etc.) and surface state parameters (spectral albedos and radiation absorption amounts, photosynthetic and stomatal conductance rates, etc.). The corresponding relations in many cases are

complicated nonlinear functions (Sellers, 1985) and we must resort to substantial simplifications in developing algorithmss if they are to be practical. In this section, we shall discuss some of the methods that are currently in use and that may be broadly termed as algorithms.

Spectral Vegetation Indices

Spectral Vegetation Indices (SVI) are synthesized from spectral reflectance factors using a variety of techniques (Tucker, 1979). A number of SVIs have been proposed in the literature that employ various combinations (summing, differencing, ratioing, etc.) of vegetation Bidirectional Reflectance Factors at two or more wavelengths. It is not our objective to review the various indices or perform a comparative analysis here; the discussion is limited to a few indices and their utility in inferring the desired surface properties.

The most common indices are the Normalized Difference Vegetation Index and the Simple Ratio (SR). The component canopy reflectance factors invariably contain contribution from the soil or background litter. A Soil-Adjusted Vegetation Index (SAVI) was proposed by Huete (1988), which minimizes soil brightness influences on SVIs involving red and near-infrared wavelengths. In addition to minimizing the effect of background, top-of-the-atmosphere spectral radiance values must be corrected for atmospheric effects to recover the vegetation signal. One such index, the Atmospherically Resistant Vegetation Index (ARVI), was recently proposed by Kaufman and Tanré (1992) and incorporates a self-correction process for the atmospheric effect at red wavelength by utilizing the radiance difference between blue and red wavelengths. The Global Environment Monitoring Index (GEMI) was recently developed to specifically correct for atmospheric effects in AVHRR data by employing a nonlinear combination of red and near-infrared reflectances (Pinty and Verstraete, 1992a). GEMI exhibits a high atmospheric transmissivity, insensitivity to soil reflectance, with the exception of very bright soils, and is empirically representative of vegetation properties in a manner similar to the other indices.

There is substantial empirical, and in some cases theoretical, evidence that these indices are related to several vegetation parameters such as ground cover, leaf area index, radiation absorption, canopy photosynthesis, canopy conductance, etc. (Hall et al., 1992). Although these findings are highly encouraging, it must be emphasized that the information content of an index depends only on the constituent radiances (or reflectances) and that an empirical relationship does not necessarily imply a causal relationship. Vegetation indices are a convenient way of summarizing the remote observations and are useful in mapping and event detection, and in some instances of estimating surface parameters, an example of which is discussed below.

From theoretical analysis it can be shown that the normalized contrast in canopy reflectance between red and near-infrared wavelengths (NDVI) is, within some bounds, responsive to the leaf area in a canopy. Similarly, the amount of photosynthetically active radiation absorbed by the photosynthesizing tissue (FAPAR) is related to the green leaf area of the canopy. Thus, we may expect a causal relationship between NDVI and FAPAR (Asrar et al., 1984). The nature of this relationship and how it varies with respect to changes in canopy, soil, and atmospheric parameters was investigated utilizing the radiative transfer method outlined in the section entitled "Statement of The Physical Problem" (Myneni and Williams, 1993). The relationship between FAPAR and NDVI was found to be independent of pixel heterogeneity, parameterized with ground cover, clump leaf area index, and variations in leaf orientation and optical properties. On the other hand, it was sensitive to background, atmospheric, and bidirectional effects. Atmospheric and bidirectional effects may be ignored if the analysis is limited to near-nadir top-of-the-canopy NDVI. Further, if the soils are moderately reflective, background effects may also be ignored. A linear model fits the resulting relationship between FAPAR and nadir TOC NDVI very significantly ($r^2 = 0.943$, $N = 280$). The slope of this relationship is 0.8465 with an intercept of -0.1083 (cf. Myneni and Williams, 1994). This linear model or algorithm for FAPAR is valid for: (a) solar zenith angle less than 60°, (b) view zenith angles about the nadir, (c) soils or backgrounds of moderate brightness (NDVI about 0.12), (d) atmospheric optical depths less than 0.65 at 550 nm.

Ecosystem productivity models can be driven with FAPAR estimates derived from remote radiance observations. Spectral measurements from satellites must be first corrected for pixel location and converted to radiances using proper geometric restitution and calibration procedures. The TOC radiance field can then be deduced from the TOA distribution using an atmospheric correction algorithm. This has been done for 13 AVHRR images of Belgium by Veroustratete et al. (1993). The TOC NDVIs thus derived were converted to FAPAR values using the linear model described above. Such a FAPAR image of Belgium is shown in Figure 9. A fine resolution FAPAR time series restituted from the coarser empirical series through Fourier analysis was then utilized to drive a model of net ecosystem carbon exchange in a deciduous forest (Veroustraete et al., 1993).

Model Inversion

A successful model inversion allows the retrieval of several independent model parameters. An inversion may further allow the calculation of surface state variables (spectral albedos, FAPAR, etc.) from a limited set of empirical reflectance values depending on the stabil-

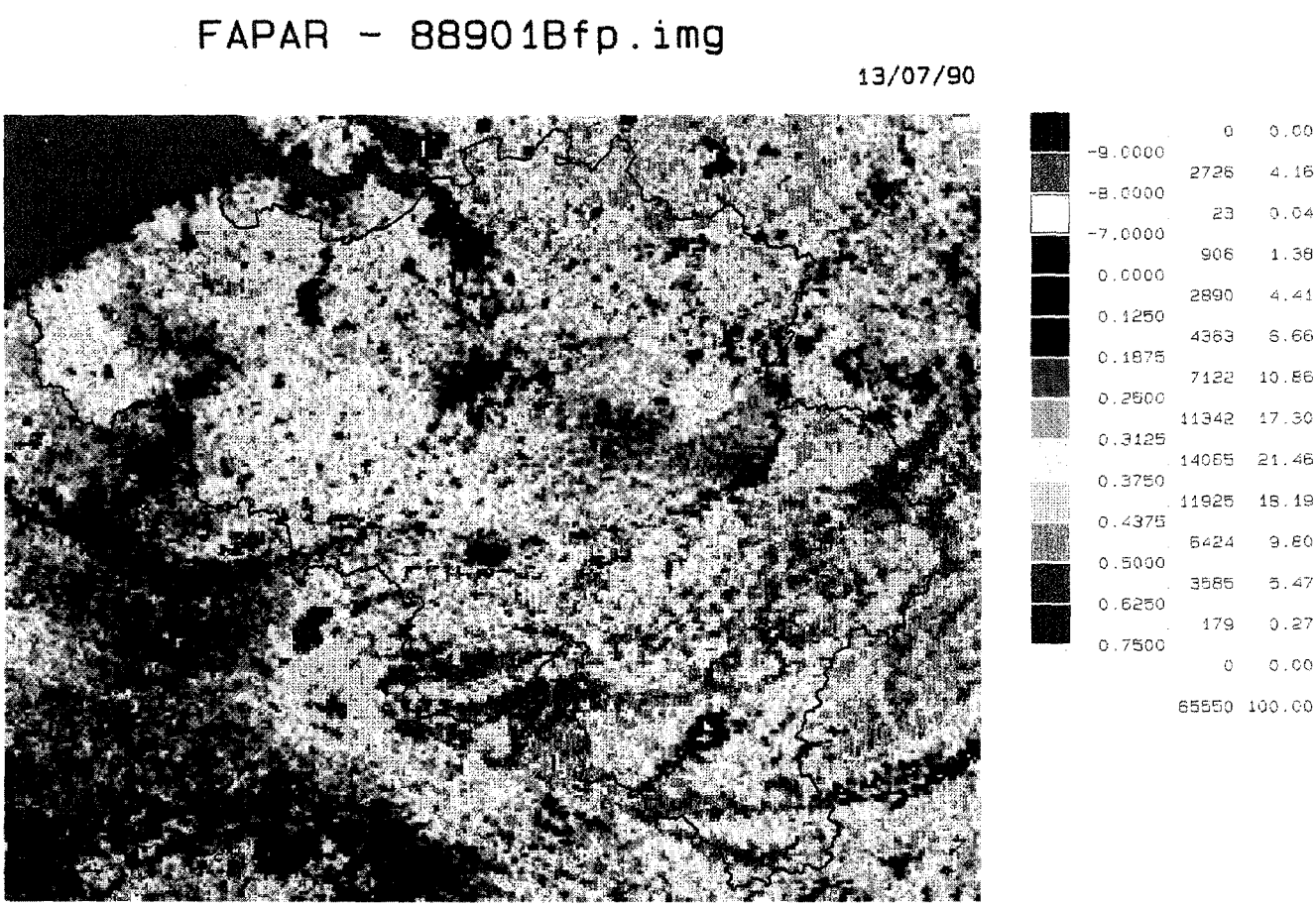

Figure 9. Map of fraction of photosynthetically active radiation absorbed by vegetation derived from atmospherically corrected AVHRR NDVI data.

ity and uniqueness of the problem. Although parameters of biological or climatological importance may be most desirable, practical limitation imposed by the number and distribution of reflectance samples, spectral regions, signal anisotrophy, and model sensitivity may dictate the optimal parameter set.

In order to infer any vegetation parameter with good accuracy, model inversion needs to be mathematically well conditioned; it implies that the partial derivatives of the bidirectional reflectance field with respect to a particular parameter has to be nonzero and should take values as high as possible. Goel and his colleagues pioneered the study of model inversions as detailed in a series of papers beginning in 1983. After developing an appropriate problem definition, merit function and inverstion strategy (Goel and Strebel, 1983), they inverted several one-dimensional models—most notably the Suits (1972), SAIL (Verhoef, 1984) and Cupid (Norman, 1979) models—and quantified parameter relationships and model sensitivity. Strahler and his colleagues developed and inverted a reflectance model that simulates a heterogeneous vegetation canopy as an assortment of geometrical objects (Li and Strahler, 1985). Antyufeev and Marshak (1990) developed a radiative transfer model and inverted it using Monte Carlo techniques. They retrieved three optical and four geometrical canopy parameters from reflectance data at two wavelengths. The hybrid three-dimensional model developed by Welles and Norman (1991) combines the geometrical objects and radiative transfer approaches to simulate the reflectance of heterogeneous vegetation canopies. This model has been inverted by Goel somewhat less successfully (Goel, 1992, personal communication). Recently, simple analytical models have been developed and inverted specifically for application to climate models (Dickinson et al., 1990; Pinty et al., 1990). General discussion on model inversion and some central ideas are concisely summarized in Privette et al. (1994).

The general inversion problem may be stated as follows: given a set of empirical directional reflectance measurements, determine the set of independent model parameters such that the computed directional reflectances best fit the empirical directional reflectances.

The fit of the empirical data is determined by the merit function (Goel and Strebel, 1983), ε^2, defined as

$$\varepsilon^2 = \sum_{j=1}^{n} (r_j - r_{jm})^2 \qquad (21)$$

where r_j is the directional reflectance for a given scan and solar angle geometry, r_{jm} is the geometrically analogous model estimate, and n is the number of reflectance samples. A penalty function may be used to limit the independent parameter space to physically possible values. For instance, the sum of leaf reflectance and transmittance can be constrained, based on physical arguments, to be ≤ 1. The ability to correctly determine target parameters through model inversion therefore depends on the dataset $\{r_{jm}\}$, the likeness of the model to physical reality and ability of the optimization algorithm chosen to minimize Eq. (21) over the parameter space.

There are several methods for minimizing the merit function and the choice of a particular method depends on the mathematical properties of the function to be minimized. Three commonly used minimization routines are: the downhill simplex method used by Privette et al. (1993) (subroutine AMOEBA from Press et al., 1986), the conjugate direction set method used by Kuusk (1991) (subroutine POWELL from Press et al., 1986), and a quasi-Newton method used by Pinty et al. (1990) (subroutine E04JAF from Numerical Algorithms Group). These three routines do not require evaluation of function derivatives for minimization. This is particularly appealing for complex, nonlinear formulations, such as those used in canopy reflectance modelling.

In practice, measured data are contaminated with noise from various sources. In the context of model inversion, the question of the impact of noise on the accuracy of the parameters retrieved must be addressed. These effects can be analyzed using synthetic data sets, that is, model-generated data, where a Gaussian noise of zero mean and known standard deviation is added to the data (Pinty et al., 1990).

As mentioned above, model inversions are performed using Eq. (21) with an optimization routine provided by standard libraries [*E04JAF* from the Numerical Algorithm Group for solving the nonlinear system with a quasi-Newton scheme, and *RAN 1, GASDEV* from Numerical Recipes (Press et al., 1986) for the generation of random noise]. A number of synthetic noisy data sets can be created depending on the conditions used to select the random noise series. The retrieved values for each of the model parameters can be averaged, which leads to an evaluation of the behavior of the inversion procedure with respect to noisy data sets. A critical issue when performing such an analysis is the randomness of the series of generated numbers, which in turn depends on the seed values used in the procedure. To illustrate this aspect, we considered two different cases by changing the seed values applied to the Numerical Recipes

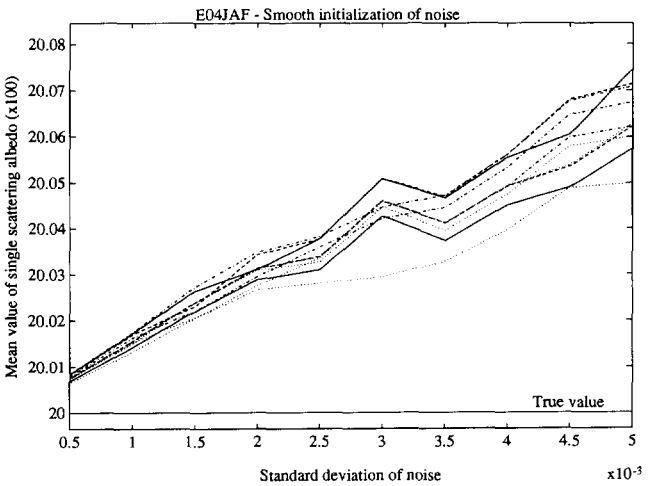

Figure 10a. Mean values of the single scattering albedo as a function of the standard deviation of the noise in the input data. For a given level of noise, each value corresponds to an average of 100 inversions performed by changing the seed according to a regular progression of negative integer numbers (Case 1). The same noise generator is used with changing values in the standard deviation of the noise.

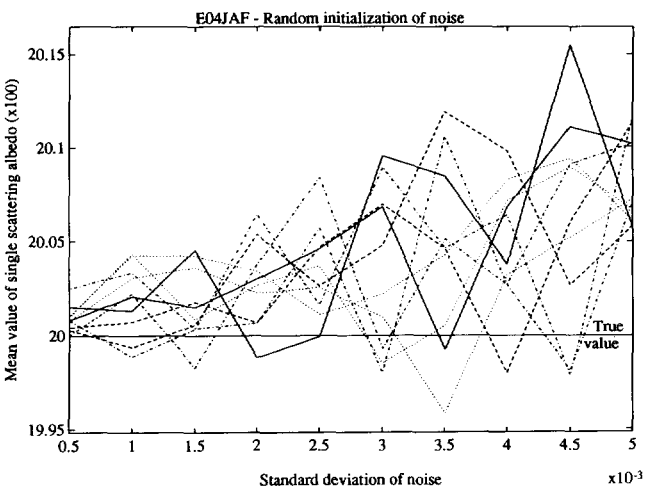

Figure 10b. Same as Figure 10a except that the seeds are randomly distributed both for a given level of noise and standard deviation of the noise (Case 2).

algorithm—the seeding series given by a regular progression of negative integer numbers (Case 1) and by a series of a priori random integer values obtained from a different external routine (Case 2). Figures 10a and 10b show the results of these two methods for a sensitive vegetation parameter, the single scattering albedo. The mean quantities reported are averages over 100 individual values, each of these corresponding to the retrieval made using the same level of noise but with a different seed as indicated above. The results obtained in Case 1 indicate a systematic overestimation of this model parameter with increasing noise level and, the smooth-

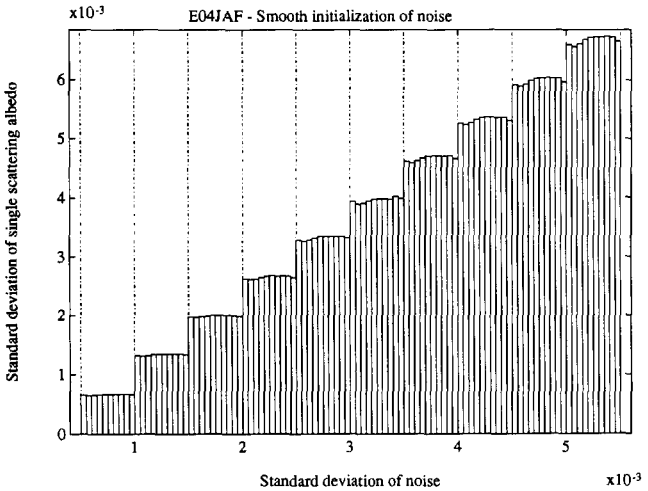

Figure 10c. Distribution of the standard deviations corresponding to the mean single scattering albedos obtained when performed 100 inversions, given as a function of the standard deviation of the noise in the input data (Case 1).

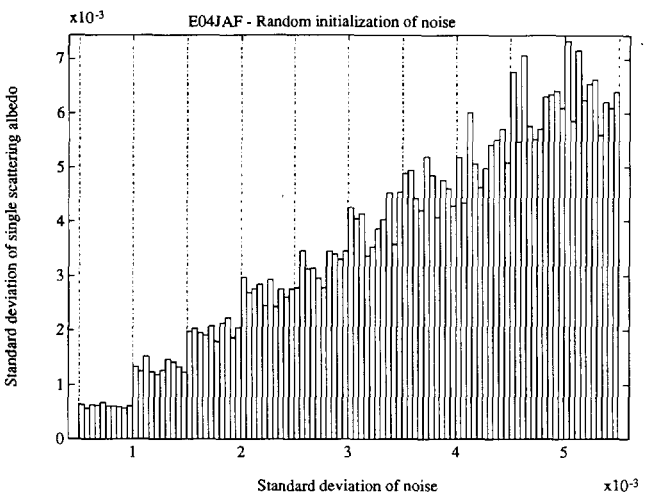

Figure 10d. Same as Figure 10c; (Case 2).

ness of the plotted curves is clearly noticeable. By contrast, Case 2 leads to much more variable and nonmonotonic features regarding the relationship between the noise level and the average retrieved single scattering albedo. For the same two cases, Figures 10c and 10d show the standard deviation corresponding to each of the ten retrievals made at a given noise level, plotted as a function of this noise level. Both figures depict a quasi-linear relationship between the standard deviation in the input noise and the standard deviation in the retrieved single scattering albedo values. In Case 2, the distribution of the standard deviation values at a given level of input noise appears to be more *noisy* than in Case 1.

Inversion of empirical data with a one-dimensional radiative transfer model (Shultis and Myneni, 1988) is

Table 3. True and Mean Retrieved Parameter Values with Standard Deviations for Soybean Data of 27 Aug. 1980.

	True	*Retrieved*	
Parameter	μ	μ	σ
LAI (both channels)	2.9	4.1	2.5
LAI (red only)		5.4	2.4
LAI (NIR only)		2.8	1.9
Leaf refl. (NIR)	0.454	0.495	0.067
Leaf refl. (red)	0.073	0.089	0.006
Leaf trans. (NIR)	0.518	0.376	0.055
Leaf trans. (red)	0.064	0.070	0.028
Soil refl. (NIR)	0.232	0.418	0.127
Soil refl. (red)	0.143	0.133	0.045
μ (Beta LAD)	1.61	1.54	0.502
v (Beta LAD)	2.18	2.52	1.03

Unless otherwise noted, retrieved values were averaged over all 12 datasets and both channels. True LAD parameter values are from Goel and Strebel (1983).

illustrated with the soybean data collected by Ranson et al. on 27 August 1988 (Privette et al., 1993). Data from two spectral bands, 0.6–0.7 μm (red) and 0.8–1.1 μm (NIR), were used in the inversion. The downhill simplex method was used for minimizing the merit function. The mean and standard deviations of the retrieved parameters are shown in Table 3. The mean retrieved LAI is high, although the measured value is within one standard deviation. Closer inspection reveals that the red LAI estimate is high but the NIR estimate is excellent (0.1 absolute error). The coefficients of the Beta distribution are close to the true values and suggest a predominantly erectophile canopy. Estimates of leaf reflectance were reasonable though slightly high. Although the red reflectance value differed by just 0.016 absolute, the measured value was outside the one standard deviation confidence interval. The NIR value differed by 0.041 but was within the confidence interval. Leaf transmittance was overestimated by 0.006 in the red and underestimated by 0.142 in the NIR. The red soil reflectance estimate was excellent (5% relative error). The NIR estimate was high (80% relative error).

At the present time, inversion of physical models is more of an art than exact science. Several topics in inversion studies need to be investigated before an operational scheme can be proposed. Some of these include (1) alternate forms of the merit function and their mathematical properties, (2) optimum number of parameters for retrieval, (3) optimal sampling schemes, (4) the importance of noise in the measurements, (5) success in parameter retrieval at various wavelengths, (6) starting points, (7) nesting of models of varying accuracy in an inversion scheme and (8) definition of a successful inversion. Furthermore, the competing advantages of computational efficiency and physical reality should dictate some optimum level of model sophistica-

tion. This threshold presently has not been determined and undoubtedly will change with technical improvements.

Expert System

Conventional algorithms such as those based on spectral indices for inferring surface hemispherical reflectance, percentage of ground cover, biomass, leaf area index, photosynthetic capacity, etc. are static and limited in scope. These algorithms cannot deal with the variability inherent in remote sensing data (e.g., variable off-nadir viewing capabilities, varying solar zenith angles, various sensor wavelengths, cloud cover problems, missing data, atmospheric effects, etc.). Information extraction systems, at a minimum, must be designed with these factors in mind. In addition, it is desirable to obtain an estimate of the accuracy of inference. Moreover, systems must be flexible enough to handle decisions at the expert's level.

In the recent years an expert system called VEG was developed with the above in mind (Kimes et al., 1991, 1992). The current version of VEG is a powerful system for inferring vegetation characteristics using nadir and/or directional reflectance data as input. VEG is also a powerful tool for aiding a researcher in developing new and more accurate techniques for inferring vegetation characteristics as well as testing these techniques. Finally, VEG has options to process files of remotely sensed data collected over large regions of the earth.

Part of VEG is designed to have any array of extraction techniques for inferring vegetation characteristics using nadir and/or directional reflectance data as input. Currently, the system has many techniques for inferring spectral hemispherical reflectance, percentage of ground cover and view angle extension. It is designed to be easily expanded to handle other inferences, such as total hemispherical reflectance, leaf area index, biomass, photosynthetic capacity, etc. The system intelligently and efficiently integrates traditional spectral data with diverse knowledge bases available in the literature, from field data sets of directional scattering behavior, and from human experts. VEG accepts any combination of nadir and/or off-nadir spectral data of an unknown target as input, determines the best strategy(s) for inferring the desired vegetation characteristic, applies the strategy(s) to the target data, and provides a rigorous estimate of the accuracy of the inference. Several research applications using VEG have been made (Kimes and Deering, 1992; Kimes and Holben, 1992; Kimes et al., 1993a, 1993b).

Neural Networks and Genetic Algorithms

Recently, some new approaches to the extraction of scene parameters from optical remote sensing data have been developed by combining physically based models and measurements with neural computing techniques. Ishimaru et al. (1990) outlined the basic approach of employing a backpropagation neural network to invert atmospheric particle size distribution parameters from optical data. Smith (1993) first trained a backpropagation neural network to invert a simple multiple scattering model to estimate leaf area index from reflectance at three wavelengths and then subsequently applied the trained network to satellite observations. He reported estimated errors of less than 30% and indicated that the method appeared to be much less sensitive to initial guesses for the parameters than other inversion techniques. A potential drawback to the technique is the difficulty of interpreting the network weights, although Smith (1993) discussed the use of a genetic algorithm to map the decision boundaries of the inversion.

CONCLUDING REMARKS

Models of varying degree of sophistication describing most of the known physical mechanisms are available in the literature. However, research is required in the area of modeling tree architecture, especially for coniferous species, and quantifying spatial heterogeneity at the landscape level. Further simplification of most models is required if they are to be utilized in the analysis of satellite data. The information content of remotely sensed data may be conceptually ordinated along the temporal, spatial, spectral and directional (and, polarization) dimensions. Algorithms must be devised to exploit the full information content in the signal. The state-of-the-art is far from satisfactory. In spite of obvious limitations, spectral vegetation indices are still preferable in the analysis of large spatial scale data sets. The promise of remote sensing, however, lies in those methods that utilize physical models and advances in computer science and technology.

This work was made possible with the financial support of NASA grant NAS5-30442 to RBM and DLW. The sections Bidirectional Effects and Neural Networks and Genetic Algorithms are contributions of Drs. R. Dubayah and J. A. Smith, respectively, and we gratefully acknowledge their participation. JLP is a DOE Global Change Graduate Fellow. Most of this manuscript was prepared at the Blaise Pascal University in France; JLP and RBM acknowledge the hospitality and support of the Laboratoire de Météorologie Physique in Clermont-Ferrand.

REFERENCES

Antyufeev, V. S., and Marshak, A. L. (1990), Inversion of a Monte Carlo model for estimating vegetation canopy parameters, *Remote Sens. Environ.* 23:201–209.

Asrar, G., Fuchs, M., Kanemasu, E. T., and Hatfield, J. H. (1984), Estimating absorbed photosynthetic radiation and

leaf area index from spectral reflectance in wheat, *Agron. J.* 76:300–306.

Asrar, G., Myneni, R. B., Li, Y., and Kanemasu, E. T. (1989), Measuring and modelling spectral characteristics of a tall-grass prairie, *Remote Sens. Environ.* 27:143–155.

Borel, C. C., and Gerstl, S. A. W., and Powers, B. J. (1991), The radiosity method in optical remote sensing of structured 3-D surfaces, *Remote Sens. Environ.* 36:13–44.

Deepak, A., and Gerber, H. E. (Eds.) (1983), *Report of WMO (CAS)/Radiation (Williamsburg, Virginia, USA,* 28–30 March, 1983), World Meteorological Organisation, Geneva, Report No. WCP-55.

Dickinson, R. E., Pinty, B., and Verstraete, M. M. (1990), Relating surface albedos in GCM to remotely sensed data, *Agric. For. Meteorol.* 52:109–132.

Diner, D. J., and Martonchik, J. V. (1984), Atmospheric transfer of radiation above an inhomogeneous Non-Lambertian reflecting ground. II. Computational considerations and results, *J. Quant. Spectroscp. Radiat. Transfer*, 32:279–304.

Dozier, J. (1989), Spectral signature of alpine snow cover from the Landsat Thematic Mapper, *Remote Sens. Environ.* 28: 9–22.

Dubayah, R. (1992), Estimating net solar radiation using Landsat Thematic Mapper and digital elevation data, *Water Resources Res.* 28:2469–2484.

Ganapol, B. D., and Myneni, R. B. (1992), The F_N method for the one-angle radiation transfer equation applied to plant canopies. *Remote Sens. Environ.* 39:213–231.

Goel, N. S. (1988), Models of vegetation canopy reflectance and their use in estimation of biophysical parameters from reflectance data, *Remote Sens. Rev.* 4:1–222.

Goel, N. S., Rozenhal, I., and Thompson, R. L. (1991), A computer graphics based model for scattering from objects of arbitrary shapes in the optical region, *Remote Sens. Environ.* 36:73–104.

Goel, N. S., and Strebel, D. E. (1983). Inversion of vegetation canopy reflectance models for estimating agronomic variables. I: Problem definition and initial results using the Suits' model, *Remote Sens. Environ.* 13:487–507.

Hall, F. G., Huemmrich, K. F., Goetz, S. J., Sellers, P. J., and Nickeson, J. E. (1992), Satellite remote sensing of surface energy balance: Success, failures, and unresolved issues in FIFE, *J. Geophys. Res.* 97:19,061–19,089.

Huete, A. R. (1988), A Soil-adjusted vegetation index (SAVI), *Remote Sens. Environ.* 25:295–309.

Ishimaru, A., Marks, R. J., Tsang, L., Lam, C. M., and Park, D. C. (1990), Particle size distribution determination using optical sensing and neural networks, *Opt. Lett.* 25:1221–1223.

Jacquemoud, S., and Baret, F. (1990), PROSPECT: A model of leaf optical properties spectra, *Remote Sens. Environ.* 34: 75–91.

Jacquemoud, S., Baret, F., and Hanocq, J. F. (1992), Modelling spectral and bidirectional soil reflectance, *Remote Sens. Environ.* 41:123–132.

Jupp, D. L. B., Walker, J., and Penridge, L. K. (1986), Interpretation of vegetation structure in Landsat MSS imagery: a case study in disturbed semi-arid eucalypt woodlands. Part 2. Model-based analysis. *J. Environ. Manage.* 23:35–57.

Kaufman, Y. J. (1989), The atmospheric effect on remote sensing and its corrections, in *Theory and Applications of Optical Remote Sensing* (G. Asrar, Ed.), J. Wiley, New York, pp. 336–428.

Kaufman, Y. J., and Tanré, D. (1992), Atmospherically resistant vegetation index (ARVI) for EOS-MODIS, *IEEE Trans. Geosci. Remote Sens.* 30:261–270.

Kimes, D.S., and Deering, D. W. (1992), Remote sensing of surface hemispherical reflectance (albedo) using pointable multi-spectral imaging spectrometers, *Remote Sens. Environ.* 39:85–94.

Kimes, D. S., and Holben, B. N. (1992), Extracting spectral albedo from NOAA 9 AVHRR multiple view data using an atmospheric correction procedure and an expert system, *IEEE Trans. Geosci. Remote Sens.* 13:275–289.

Kimes, D. S., Harrison, P. R., and Ratcliffe, P. A. (1991), A Knowledge-based expert system for inferring vegetation characteristics, *Int. J. Remote Sens.* 12:1987–2020.

Kimes, D. S., Harrison, P. R., and Harrison, P. A. (1992), Learning class descriptions from a data base of spectral reflectance with multiple view angles, *IEEE Geosci. Remote Sens.* 30:315–325.

Kimes, D. S., Irons, J. R., and Levine, E. R. (1993a), Learning class descriptions from a data base of spectral reflectance of soil samples, *Remote Sens. Environ.* 43:161–169.

Kimes, D. S., Kerber, A. G., and Sellers, P. A. (1993b), Spatial errors in creating hemispherical reflectance (albedo) maps from directional reflectance data, *Remote Sens. Environ.* 43:1–10.

Knyazikin, Y., and Marshak, A. L. (1991), Fundamental equations of radiative transfer in leaf canopies and iterative methods of their solution, In *Photon-Vegetation Interactions: Applications in Optical Remote Sensing and Plant Ecology* (R. B. Myneni and J. Ross, Ed.), Springer-Verlag, Heidelberg, Germany, pp. 9–44.

Knyazikhin, Y. V., Marshak, A. L., and Myneni, R. B. (1992), Interaction of photons in a canopy of finite dimensional leaves, *Remote Sens. Environ.* 39:61–74.

Kuusk, A. (1985), The hot spot effect of a uniform vegetative cover, *Sov. J. Remote Sens.* 3:645–658.

Kuusk, A. (1991), The determination of vegetation canopy parameters from optical measurements, *Remote Sens. Eniviron.* 37:207–218.

Li, X., and Strahler, A. H. (1985), Geometrical-optical modelling of a conifer forest canopy, *IEEE Trans. Geosci. Remote Sens.* GE-23:705–721.

Marshak, A. L. (1989), The effect of the hot spot on the transport equation in plant canopies, *J. Quant. Spectroscop. Radiat. Transfer*, 42:615–630.

Myneni, R. B., and Asrar, G. (1991), Photon interaction cross sections for aggregations of finite dimensional leaves, *Remote Sens. Environ.* 37:219–224.

Myneni, R. B., and Asrar, G. (1993), Radiative transfer in three dimensional atmosphere vegetation media, *J. Quant. Spectroscp. Radiat. Transfer*, 49:585–598.

Myneni, R. B., and Ganapol, B. D. (1991), A simplified formulation of photon transport in leaf canopies with finite dimensional scatterers, *J. Quant. Spectroscp. Radiat. Transfer* 46: 135–140.

Myneni, R. B., and Ross, J. (eds.) (1991), *Photon-Vegetation Interactions: Applications in Optical Remote Sensing and Plant Ecology*, Springer-Verlag, Heidelberg, Germany.

Myneni, R. B., and Williams, D. L. (1994), On the relationship

between FAPAR and NDVI, *Remote Sens. Environ.* 49: 200–211.

Myneni, R. B., Asrar, G., and Gerstl, S. A. W. (1990), Radiative transfer in three dimensional leaf canopies, *Trans. Theory Stat. Phys.* 19:205–250.

Myneni, R. B., Asrar, G., and Hall, F. G. (1992), A three dimensional radiative transfer model for optical remote sensing of vegetated land surfaces, *Remote Sens. Environ.* 41:85–103.

Myneni, R. B., Gutschick, V. P., Asrar, G., and Kanemasu, E. T. (1988), Photon transport in vegetation canopies with anisotropic scattering: Parts II and IV, *Agric. For. Meteorol.* 42:17–40 & 42:101–120.

Myneni, R. B., Marshak, A. L., and Knyazikhin, Yu. (1991), Transport theory for leaf canopies with finite dimensional scattering centers, *J. Quant. Spectroscp. Radiat. Transfer*, 46:259–280.

Nilson, T., and Kuusk, A. (1989), A reflectance model for the homogeneous plant canopy and its inversion, *Remote Sens. Environ.* 27:157–167.

Norman, J. M. (1979), Modelling of complete crop canopy, In *Modification of the Aerial Environment of Plants* (B. G. Barfield and J. F. Gerber, Eds.), ASE Monograph No. 2, St. Joseph, Michigan, pp. 249–277.

Pinty, B., and Verstraete, M. M. (1992a), GEMI: A non-linear index to monitor global vegetation from satellites, *Vegetatio* 101:15–20.

Pinty, B., and Verstraete, M. M. (1992b), On the design and validation of surface bidirectional reflectance and albedo models, *Remote Sens. Environ.* 41:155–167.

Pinty, B., Verstraete, M. M., and Dickinson, R. E. (1989), A physical model for predicting bidirectional reflectance over bare soil, *Remote Sens. Environ.* 27:273–288.

Pinty, B., Verstraete, M. M., and Dickinson, R. E. (1990), A physical model for the bidirectional reflectance of vegetation canopies—Part 2: Inversion and validation, *J. Geophys. Res.* 95:11767–11775.

Press, W. H., Flannery, B. P., Teukolsky, S. A., and Vetterling, W. T. (1986), *Numerical Recipes*, Cambridge Univ. Press, New York, pp. 274–312.

Privette, J. L., Myneni, R. B., Tucker, C. J., and Emery, W. J. (1994), Invertibility of a 1-D discrete ordinates canopy reflectance model, *Remote Sens. Environ.* 48:89–105.

Ranson, K. J., and Biehl, L. L. (1983), *Corn Canopy Reflectance Modelling Data Set*, LARS Tech. Rep., Purdue Univ., W. Lafayette, Indiana 47907, USA.

Ross, J. (1981), *The Radiation Regime and Architecture of Plant Stands*, Dr. W. Junk Publ., Den Haag, The Netherlands.

Sellers, P. (1985), Canopy reflectance, photosynthesis and transpiration, *Int. J. Remote Sens.* 8:1335–1372.

Shultis, J. K., and Myneni, R. B. (1988), Radiative transfer in vegetation canopies with anisotropic scattering, *J. Quant. Spectroscp. Radiat. Transfer* 39:115–129.

Smith, J. A. (1993), LAI inversion using a backpropagation neural network trained with a multiple scattering model, *IEEE Trans. Geosci. Remote Sens.* GE-31: (In Press).

Stewart, R. (1990), *Modelling Radiant Energy Transfer in Vegetation Canopies*, M. S. Thesis, Kansas State University, Manhattan, Kansas 66506.

Strebel, D. E., Goel, N. S., and Ranson, K. J. (1985), Two-dimensional leaf orientation distributions, *IEEE Trans. Geosc. Remote Sens.* GE-23:640–647.

Suits, G. W. (1972), The calculation of the directional reflectance of a vegetative canopy, *Remote Sens. Environ.* 2: 117–125.

Tanré, D., Deroo, C., Duhaut, P., Herman, M., Morcrette, J. J., Perbos, J., and Deschamps, P. Y. (1990), Description of a computer code to simulate the satellite signal in the solar spectrum: the 5S code, *Int. J. Remote Sens.* 11:659–668.

Tucker, C. J. (1979), Red and photographic infrared linear combinations for monitoring vegetation, *Remote Sens. Environ.* 8:127–150.

Vanderbilt, V. C., and Grant, L. (1985), Plant canopy specular reflectance model, *IEEE Trans. Geosc. Remote Sens.* GE-23: 722–730.

Verhoef, W. (1984), Light scattering by leaf layers with application to canopy reflectance, *Remote Sens. Environ.* 16: 125–141.

Veroustraete, F., Patyn, J., Van Rensbergen, J., Kretzschmar, J., and Myneni, R. B. (1993), *Coupling of Remote Sensing Data with a Simple Ecosystem Model to Estimate Photosynthetic Assimilation*, Report ENE.RA9307, Flemish Institute for Technological Research, Mol, Belgium.

Verstraete, M. M., Pinty, B., and Dickinson, R. E. (1990), A physical model of the bidirectional reflectance of vegetation canopies. 1. Theory, *J. Geophys. Res.* 95:11755–11765.

Welles, J. M., and Norman, J. M. (1991), Photon Transport in Discontinuous Canopies: A Weighted Random Approach, In *Photon-Vegetation Interactions: Applications in Optical Remote Sensing and Plant Ecology* (R. B. Myneni and J. Ross, Eds.), Springer-Verlag, Heidelberg, Germany, pp. 389–414.